HHS Public Access

Author manuscript

Cancer Lett. Author manuscript; available in PMC 2025 November 03.

Published in final edited form as:

Cancer Lett. 2025 November 01; 632: 217977. doi:10.1016/j.canlet.2025.217977.

Restricting metabolic plasticity enhances stress adaptation through the modulation of PDH and HIF1A in TRAP1-depleted colon cancer

Hong-Yuan Tsai[a,*], **Miao-Hsueh Chen**[b], **Jihye Yun**[c], **Lisa A. Lai**[d], **John F. Valentine**[e], **Mary P. Bronner**[f,g], **Teresa A. Brentnall**[d], **Sheng Pan**[h,i], **Ru Chen**[a,*]

[a]Section of Gastroenterology and Hepatology, Department of Medicine, Baylor College of Medicine, Houston, TX, USA

[b]USDA/ARS, Children's Nutrition Research Center, Department of Pediatrics, Baylor College of Medicine, Houston, TX, USA

[c]Department of Genetics, Division of Basic Science Research, The University of Texas MD Anderson Cancer Center, Houston, TX, USA

[d]Department of Medicine, University of Washington, Seattle, WA, USA

[e]Division of Gastroenterology, Hepatology and Nutrition, Department of Medicine, University of Utah, Salt Lake City, UT, USA

[f]Department of Pathology, University of Utah, Salt Lake City, UT, USA

[g]Huntsman Cancer Institute, University of Utah, Salt Lake City, UT, USA

[h]Brown Foundation Institute of Molecular Medicine, University of Texas Health Science Center at Houston, Houston, TX, USA

[i]Department of Integrative Biology and Pharmacology, McGovern Medical School, University of Texas Health Science Center at Houston, Houston, TX, USA

Abstract

Metabolic plasticity allows cancer cells to survive under adverse conditions. To investigate the role of mitochondrial chaperone tumor necrosis factor receptor-associated protein 1 (TRAP1)

*Corresponding authors. Baylor College of Medicine. 1 Baylor Plaza, Houston, TX, 77030, USA. hong-yuan.tsai@bcm.edu (H.-Y. Tsai), ru.chen@bcm.edu (R. Chen).

Declaration of competing interest

The authors declare that they have no known competing financial interests or personal relationships that could have appeared to influence the work reported in this paper.

CRediT authorship contribution statement

Hong-Yuan Tsai: Writing – review & editing, Writing – original draft, Validation, Methodology, Investigation, Formal analysis, Data curation, Conceptualization. **Miao-Hsueh Chen:** Writing – review & editing, Supervision, Methodology, Investigation, Data curation. **Jihye Yun:** Writing – review & editing, Resources. **Lisa A. Lai:** Writing – review & editing, Resources, Investigation. **John F. Valentine:** Writing – review & editing, Resources, Conceptualization. **Mary P. Bronner:** Writing – review & editing, Resources, Conceptualization. **Teresa A. Brentnall:** Writing – review & editing, Visualization, Resources, Conceptualization. **Sheng Pan:** Writing – review & editing, Resources, Methodology, Investigation, Formal analysis, Data curation, Conceptualization. **Ru Chen:** Writing – review & editing, Visualization, Supervision, Funding acquisition, Data curation, Conceptualization.

in this process, we used CRISPR/Cas9 mediated genetic deletion to knock out (KO) TRAP1 in colon cancer cells. Depletion of TRAP1 triggered a series of events: induced metabolic reprogramming, increased glycolytic flux, downregulation of mitochondrial complex I, and elevated ROS generation. TRAP1-deficient cells showed tolerance to Oxidative Phosphorylation (OXPHOS) inhibitors and exhibited a higher extracellular acidification rate (ECAR). Additionally, TRAP1 depletion activated hypoxia response elements (HREs) and upregulated HIF1A target genes such as GLUT1 and MCT1. Furthermore, pyruvate dehydrogenase kinases 1 (PDK1) was upregulated in KO cells, leading to the inactivation of the tricarboxylic acid (TCA) cycle enzyme, pyruvate dehydrogenase (PDH). This metabolic shift towards glycolytic metabolism resulted in increased glycolytic metabolism, elevated lactic acid production, and higher glucose consumption, making TRAP1-depleted cancer cells more dependent on this altered metabolism for survival. Treatment with DCA, a PDK inhibitor, restored PDH activity, exacerbated oxidative stress, and increased cell death in KO cells. Our study here sheds light on how TRAP1 depletion affects metabolic plasticity, driving colon cancer cells to adapt to metabolic and oxidative stress. These findings highlight TRAP1 as a promising therapeutic target for manipulating metabolic plasticity and overcoming drug resistance in cancer therapy.

Keywords

TRAP1; Metabolism; Mitochondria; ROS; HIF1A; PDH

1. Introduction

Colorectal cancer (CRC), the second leading cause of cancer-related deaths, is linked to disrupted metabolic pathways that contribute to its progression [1,2]. During tumorigenesis, rapidly dividing cancer cells encounter a harsh environment characterized by nutrient scarcity, potential drug exposure, and oxygen availability. To survive, CRC cells adapt by altering their metabolic pathways to provide the energy required for proliferation and developing drug resistance [3]. A promising avenue for improving treatment outcomes involves understanding how cancer cells reprogram their metabolism to support growth. Metabolic reprogramming is recognized as a hallmark of cancer, not only promoting tumor development [4,5], but also contributing to resistance against chemotherapeutic agents [6]. Research indicates that cancer cells often display metabolic plasticity rather than dependency, allowing them to switch between glycolytic bioenergetics and mitochondrial bioenergetics depending on environmental context [7,8]. Throughout tumor progression, this metabolic plasticity enables cancer cells to maintain a metabolic hybrid, thereby supporting their energy needs to survive in stressful environments [9]. Metabolic plasticity of cancer cells offers a valuable opportunity for developing new anti-cancer therapies. Targeting metabolic enzymes such as mitochondrial pyruvate dehydrogenase (PDH) or glutaminase has shown promise, with some strategies already in clinical trials [10,11].

Mitochondria, the cell's powerhouse for energy production, plays a prominent role in maintaining a cancer cell's metabolic profile. Disrupting mitochondrial function with mitochondrial HSP90 inhibitor Gamitrinib can limit this metabolic plasticity by inducing mitochondrial dysfunction and impairing energy production, thereby enhancing

the effectiveness of MAPK inhibitor treatments [12]. Even when oxygen is sufficient, cancer cells often prefer glycolysis over pyruvate oxidation to fulfill biosynthetic and redox needs, a phenomenon known as aerobic glycolysis [13–15]. For redox homeostasis, Reactive Oxygen Species (ROS) reduces pyruvate oxidation via stabilization of the HIF1A transcription factor to facilitate glycolysis in an oxidative stress environment [16–18]. In addition, HIF1A suppresses oxidative phosphorylation through NDUFA4L2, inhibiting electron transport chain complex I activity and ROS generation [19]. HIF1A downstream genes, such as GLUT1, GLUT3, and MCTs, promote glycolytic bioenergetics by increasing glucose uptake and lactate exportation [20–22]. Under hypoxic conditions, glycolytic gatekeeper dehydrogenase kinase 1 (PDK1) is activated by HIF1A. The activation of PDK1 suppresses mitochondrial functions by phosphorylating the pyruvate dehydrogenase (PDH) E1α subunit, thereby inhibiting the PDH complex (PDC). PDH is the essential rate-limiting step connecting glycolysis with the TCA cycle, which converts pyruvate to acetyl-CoA within the mitochondrial matrix. The inhibition of PDH reduces pyruvate oxidation via the tricarboxylic acid (TCA) cycle [23]. In this regard, regulation of the PDH complex by PDKs is critical for mitochondrial respiration and metabolic plasticity [24]. Restoring PDH activity using the PDK inhibitor DCA shifts metabolism from glycolysis to mitochondrial respiration and suppresses colon cancer growth [25].

TRAP1, a heat shock protein localized in the mitochondria [26–28], is frequently dysregulated in various cancers, including colorectal cancer [29–34]. TRAP1 is involved in various cellular processes, including regulation of metabolic energy, ROS detoxification, and promoting cell survival [35–37]. Our previous studies have shown that TRAP1 is upregulation during the neoplastic progression of colitis-associated colorectal cancer [38–40]. Inhibition of TRAP1 by gamitrinib-triphenylphosphonium (G-TPP) has been found to induce cell death in multiple cancers [41–45], and restore drug sensitivity in resistant cell lines [46–48]. Targeting NRF2, a key regulator of cellular stress responses, could further enhance the effectiveness of G-TPP in colorectal cancer treatment [49]. However, the role of TRAP1 in regulating the metabolic switch between aerobic glycolysis and oxidative phosphorylation in tumor cells remains poorly understood [50]. Some studies suggest that TRAP1 inhibits mitochondrial oxidative phosphorylation (OXPHOS) by binding to succinate dehydrogenase (SDH), a crucial enzyme in complex II, thereby altering energy metabolism [51,52]. This inhibition leads to intracellular succinate accumulation and HIF1A activation, promoting a metabolic shift towards aerobic glycolysis in tumor cells. Recent findings reveal a novel relationship between TRAP1 and HIF1A: under hypoxic conditions in zebrafish embryos, HIF1A stabilization enhances TRAP1 expression [53]. Conversely, TRAP1 depletion in TRAP1−/− mice results in deregulated mitochondrial respiration and a metabolic switch towards aerobic glycolysis, characterized by increased glucose consumption and lactic acid production [54]. These seemingly contradictory findings highlight the complexity and multifaceted nature of TRAP1 in regulating metabolic plasticity and drug resistance in colon cancer.

In this study, we used CRISPR/Cas9 mediated genetic deletion to knock out TRAP1 in colon cancer cells, aiming to investigate TRAP1's role in cancer metabolism and survival. Using proteomics, we identified dysregulated pathways resulting from TRAP1 depletion and further explored the mechanistic roles of TRAP1 in regulating metabolic activity

in colon cancer cells. TRAP1 depletion led to a series of metabolic changes, including oxidative stress, mitochondrial remodeling, and a heightened reliance on glycolysis. Our findings indicate that TRAP1-depleted cancer cells become “addicted” to glucose, exhibiting increased activation of hypoxia response elements (HRE) and decreased pyruvate dehydrogenase (PDH) activity. Combining TRAP1 depletion with glycolytic inhibitors demonstrated synergistic suppressive effects on colon cancer cells. These results underscore the critical role for TRAP1 in maintaining metabolic hybrid through the regulation of mitochondrial activity.

2. Materials and methods

2.1. Cell lines and growth supplements

CT26 cell line was provided by Dr. Yun’s Lab at Baylor College of Medicine. HCT116, RKO, SW48 and SW480 cells were purchase from ATCC. The cell line was cultured in Dulbecco’s Modified Eagle’s Medium supplemented with 0.1 mM sodium pyruvate, 10 % fetal bovine serum, penicillin (100 U/ml), and streptomycin (100 mg/ml). Cells were cultured in a humidified atmosphere with 5 % CO2. Rotenone, oligomycin, 2DG, Trolox and PX478 were obtained from Sigma-Aldrich (St. Louis, MO, USA). TRAP1 inhibitor (G-TPP) was purchased from MedChemExpress (Monmouth Junction, NJ 08852, USA). TRAP1 CRISPR/Cas9 plasmid was obtained from Santa Cruz (Dallas, TX, USA). pCMV6 and pCMV6/TRAP1 plasmids were obtained from Origene (Rockville, MD, USA). All tissue culture reagents were obtained from Thermo Fisher (Waltham, MA, USA).

2.2. CRISPR/Cas9–mediated knockout of TRAP1

CT26 cells were seeded into six well plates (2E+05/well) overnight. Cells were co-transfected with 1.5 μg HDR plasmid and 1.5 μg TRAP1 CRISPR/Cas9 using lipofectamine LTR from Thermos Fisher (Waltham, MA, USA) for 72 h. Cells were selected with 2 μg/ml puromycin (InvivoGen, San Diego, CA, USA) for 72 h. Single cell colony was performed by series dilution and cells were consistently selected with 2 μg/ml puromycin. TRAP1 knockout efficiency was checked using western blotting and qPCR in individual clone.

2.3. Western blotting

The cells were lysed in RIPA buffer containing protease inhibitor (Thermo Fisher, Waltham, MA, USA). Nuclear part and cytoplasm part were separated by NE-PER™ Nuclear and Cytoplasmic Extraction kit (Thermo Fisher, Waltham, MA, USA) according to the manufacturer’s protocol. Western blot analysis was performed using the following antibodies: anti-TRAP1 (1:1000) from LSBio (Lynnwood, WA, USA), anti-MCT1 (1:500), anti-NDUFA10 (1:500), anti-NDUFS2 (1:500) from Santa Cruz (Dallas, TX, USA), anti-GLUT1 (1:1000), anti-HIF1A (1:1000), anti-PDH (1:1000), anti-pPDH (S293) (1:1000), anti-pPDH (S232) (1:1000), anti-Lamin B1 (1:1000), anti-PARP (1:1000), anti-CHOP (1:1000), anti-tubulin (1:5000) and anti-actin (1:5000) were obtained from Cell Signaling (Danvers, MA, USA). Acrylamide gel was purchased from Bio-Rad (Hercules, CA, USA). Iblot was obtained from Thermo Fisher (Waltham, MA, USA). The membranes were immersed in 2 % BSA in phosphate-buffered saline + Tween 20 to block non-specific background staining. The secondary antibody was horseradish peroxidase-labeled (Jackson

Immuno Research Laboratories, West Grove, PA, USA) for enhanced chemiluminescence detection. Chemical reagents for enhancing chemiluminescent were added to the membrane and the image was detected by Bio-Rad Gel Doc™ XR+.

2.4. Quantitative real-time reverse transcriptase PCR analysis

Cellular total mRNAs were extracted, and cDNA was synthesized using the ABI cDNA synthesis kit. The cDNA products were analyzed using ABI SYBR green dye and ABI quantitative real-time PCR machine (Quantstudio 7 Pro, ABI). The reaction cocktail contained primer, cDNA and 2X SYBR green qPCR master mix. The primers sequences used were as follows: mouse TRAP1 5′-ACGGACGCACCACTCAACA-3' (sense) and 5′-AGCTCCCTGCTCACATCAAAC-3' (antisense), mouse GAPDH 5′-CAAATTCAACGGCACAGTCAA-3' (sense) and 5′-GTCTCGCTCCTGGA AGATGGT-3' (antisense). The data was analyzed using ABI software.

2.5. Cell viability assay

Parental (WT) or TRAP1-depleted (KO) cells were seeded into 96-well plates overnight at a density of 5000 cells per well. Subsequently, the cells were treated with different dosages of 2DG, DCA, G-TPP, rotenone, or oligomycin for 48 h at 37 °C in a 5 % CO2 incubator. One-tenth volume of culture media containing Cell Counting Kit-8 reagent (Dojindo, Japan) was added to each well, followed by incubation at 37 °C for 2 h. Cell viability was then measured using an ELISA reader at OD450 (CLARIOstar plus, BMG LABTECH).

2.6. Mass spectrum analysis

Cells were lysed in RIPA buffer containing protease inhibitors (Thermo Fisher, Waltham, MA, USA). The cell debris was pelleted by centrifugation at 14,000×*g* for 10 min at 4 °C. The supernatant was collected, and 50 μg of protein was processed for proteomic analysis as previously described [39,55]. Briefly, the protein lysates were reduced with 10 mM DTT (Thermo Fisher, Waltham, MA, USA) at 50 °C for 1 h, followed by alkylation with 25 mM iodoacetamide (Sigma-Aldrich,St. Louis, MO, USA) at room temperature for 30 min in the dark. The proteins were precipitated by adding a 1/4 volume of 100 % (w/v) TCA (Sigma-Aldrich,St. Louis, MO, USA) and incubating on ice for 20 min. The samples were centrifuged at 14,000×*g* for 5 min at 4 °C. The pellets were rinsed twice with ice-cold acetone, followed by another centrifugation at 14,000×*g* for 10 min. The protein pellets were then air-dried and resuspended in 50 mM ammonium bicarbonate (Sigma-Aldrich,St. Louis, MO, USA). Trypsin (Thermo Fisher, Waltham, MA, USA) was added at a 1:20 ratio in two steps with a 2 h incubation in between, with vertexing every 30 min. The samples were finally incubated overnight at 37 °C. After drying completely in a Thermo Scientific™ Savant™ SpeedVac™, the samples were resuspended in 0.1 % formic acid (Sigma-Aldrich, St. Louis, MO, USA) for LC-MS/MS analysis. One microgram of each digested sample was analyzed using a Q Exactive™ HF-X Orbitrap™ mass spectrometer (ThermoFisher Scientific, Waltham, MA, USA) interfaced with an UltiMate 3000 HPLC (ThermoFisher Scientific), as described previously [56]. The MS data were then searched against the UniProt human protein database for peptide/protein identification using the Comet algorithm embedded in the Trans-Proteomic Pipeline [57,58].

2.7. Seahorse assay

The mitochondrial function of WT and TRAP1-depleted CT26 cells was measured using the Seahorse XF Cell Mito Stress Test kit (Agilent, Santa Clara, CA) and analyzed using the Seahorse XFe24 Analyzer (Agilent, Santa Clara, CA). Briefly, cells were seeded onto an Agilent XF cell culture plate (Agilent, Santa Clara, CA) at 20,000 cells/well and cultured at 37 °C in an incubator overnight. To measure mitochondrial function, cells were washed in XF base medium and then cultured in XF base medium (Agilent, Santa Clara, CA) containing 25 mM glucose, 4 mM L-glutamine, and 1 mM sodium pyruvate for 1 h at 37 °C in a non-CO2 incubator. After incubation, 5 μM Oligomycin, 5 μM FCCP, and 2 μM rotenone were loaded into ports A, B, and C of the Seahorse plate, respectively. The microplate was then loaded onto a Seahorse XFe24 Analyzer. The oxygen consumption rate was measured based on the manufacturer's protocol and presented using the XF Cell Mito Stress Test Report Generator. The data was further analyzed using Wave software.

2.8. Cell cycle analysis

WT and KO CT26 cells were prepared and stained with DAPI (40 ng/ml) (light sensitive). The samples were placed in 12 × 75 Falcon tubes and analyzed using a fluorescence-activated cell sorter (BD Biosciences, La Jolla, CA, USA). For cell-cycle analysis, 10,000 stained cells were sorted by flow cytometery and data were analyzed using the Flow JO software (BD Biosciences).

2.9. Colony forming assay

Cells (300 cells/well) were seeded into 6-well dishes overnight. The cells were then treated with Ctrl, 1.25 mM, 2.5 mM 2DG or 10 mM DCA, 20 mM DCA, or 10 nM oligomycin, 50 nM oligomycin respectively, and incubated at 37 °C incubator for 7 days. The number of cell colonies was stained with 0.5 % crystal violet at room temperature (RT) for 15 min. The colony numbers were counted, and a *t*-test was applied to evaluate statistical significance.

2.10. Reactive oxygen species generation measurement

Cells were cultured in 24-well plates overnight and then treated with different dosages of 2DG, oligomycin, rotenone, Trolox, G-TPP, and DCA for 24 h. Intracellular ROS levels in the cells were measured using the Cellular ROS Assay Kit (DeepRed) (Abcam, Cambridge, United Kingdom), after incubation with 10 μM of the kit's reagent for 30 min. Cells were collected and washed with PBS. Then, they were resuspended in PBS containing 2 % FBS. The samples were placed in 12 × 75 Falcon tubes and analyzed using a fluorescence-activated cell sorter (BD FACSCanto II). The data were then analyzed using FlowJo software.

2.11. Glucose consumption assay

Cells were grown on a 6-well plate overnight and then treated with either fresh complete medium or medium containing different dosages of 2DG, Rotenone, PX478, or Trolox. Following incubation for 24, 48, or 72 h respectively, the supernatant medium was collected, and glucose levels were quantified using a Glucose-Glo kit (Promega, Madison, WI, USA) according to the manufacturer's protocol. luminescence was read on a luminometer for

glucose level. Glucose consumption was calculated by subtracting the glucose concentration of the culture medium from non-culture medium.

2.12. Lactate production assay

Cells were grown in a 6-well plate overnight, and the medium was refreshed with complete medium or medium containing different dosages of 2DG, rotenone, PX-475, or Trolox. Following incubation for 24, 48, or 72 h, the supernatant medium was collected, and the amount of lactate was quantified using a Lactate-Glo kit (Promega, Madison, Wisconsin, USA) according to the manufacturer's protocol. Luminescence was read on a luminometer for lactate level.

2.13. Immunofluorescence staining

Cells (10000 cells/well) were seeded into 8 well chambers overnight. Culture medium was changed to fresh medium, and cells were incubated at 37 °C incubator for 24 h. The cells were fixed with 4 % paraformaldehyde at RT for 10 min. Cells were permeabilized with 0.2 % TritonX-100 RT 5 min and incubated with 2 % goat serum/0.3 M glycine for 2 h. The slide was incubated with primary antibodies GLUT1 (1:200), HIF1A (1:200), pPDH (S232) (1:200), PDK1 (1:200) (Cell signaling (Danvers, Massachusetts, USA), or MCT1 (1:200) (Santa Cruz, Dallas, TX, USA) overnight and incubated with secondary antibody anti-rabbit-488 antibody (1:400) or secondary antibody anti-mice-488 antibody (1:400) at RT for 2 h. Cells were stained with DAPI (200 ng/ml) for 5 min. The image was observed by fluorescence (ECLIPSE E800, Nikon).

2.14. HRE luciferase reporter assay

Monolayers cells were infected with the HRE Luciferase Reporter Lentivirus purchased from LipExoGen Biotech (Baltimore, MD, USA) in the presence of 8 μg/mL polybrene for 48 h. Cells were then selected with 2 μg/mL Blasticidin (InvivoGen, San Diego, CA, USA) for 3 days. Subsequently, cells containing the HRE Luciferase Reporter were seeded into 96-well plates overnight. These cells were then treated with either Ctrl or different dosages of Trolox for 18 h. An equal volume of culture media containing Cell-Glo Reagent (Promega, Madison, WI, USA) was added, and the cells were incubated for 15 min. Luminescence was then measured using a luminescence reader.

2.15. ADP/ATP measurement

Cells were grown in a 96-well plate overnight, and then treated with 1.25 mM, 2.5 mM 2DG or 10 mM, 50 mM Rotenone for 24 h.Then the culture medium was removed and 90 μl of ATP reagent was added to each well. Incubate the plate for 1 min at room temperature. Luminescence was read on a luminometer for the ATP assay (RLUA). Incubate the plate for an additional 10 min at room temperature. After 10-min incubation, read luminescence for ATP (RLUB). This measurement provides the background prior to measuring ADP. Immediately following the reading of RLUB, add 5 μl of ADP Reagent to each well and mix by tapping the plate or pipetting. After 1 min, read luminescence for ATP (RLUC). Calculate the ADP/ATP ratio using the formula. ADP/ATP ratio = (RLUC − RLUB)/RLUA. The ADP/ATP kits were purchased from Sigma (Louis, MO, USA).

2.16. Ectopic expression of TRAP1 in KO cells

The pCMV6 and pCMV6/TRAP1 plasmids were purchased from OriGene (Rockville, MD, USA) and amplified in DH5α cells. Plasmids were then extracted using QIAGEN plasmid mini kits (Hilden, Germany) and verified by agarose gel electrophoresis. CT26 cells were seeded in 6-well plates until they reached 70 % confluence. These cells were then transfected with 2 μg of either pCMV6 or pCMV6/TRAP1 plasmid for 72 h. Selection with 2 mg/ml neomycin (InvivoGen, San Diego, CA, USA) was maintained throughout the experiment. TRAP1 protein expression was confirmed by Western blotting.

2.17. Bioinformatics analysis

The GEPIA website (https://gepia.cancer-pku.cn/index.html) was used to assess the TRAP1 gene expression level in the different groups. The correlation between genes in human colon cancer samples was performed using the ENCORI website (https://rnasysu.com/encori). The enrichment analysis of proteomic data was performed using the Gene Set Enrichment Analysis (GSEA), which is a computational method that determines a set of genes shows statistically significant, concordant differences between two groups. Differentially expressed genes analysis of the proteomic data was carried out using DESeq2, with a fold change greater than 1.5 and a false discovery rate (FDR) less than 0.1 as cutoff (http://bioinformatics.sdstate.edu/idep/). Shiny GO, a tool for analyzing genes and proteins, was employed to perform GO functional annotation and biological pathway enrichment analysis on the differentially expressed genes (http://bioinformatics.sdstate.edu/go/).

2.18. Statistical analysis

For the *in vitro* studies, each experiment was performed independently at least twice. Continuous data were presented as means ± SEMs, and two-group comparisons were performed using the student's unpaired *t*-test. All statistical tests were two-sided, and $P < 0.05$ was considered to be significant. Calculated *P*-values of $P < 0.05$ (*), $P < 0.01$ (**) and $P < 0.001$ (***) were as indicated.

3. Results

3.1. TRAP1 is essential in maintaining cellular redox homeostasis and colon cancer survival

In our previous studies, we reported an overexpression of TRAP1 in the tumor tissues and precursor lesions of colitis associated colorectal cancer [39,49]. This aberrant expression of TRAP1 in colon tumors was further confirmed by an analysis of the TCGA database, which revealed significantly higher TRAP1 mRNA levels in colon tumors compared to normal adjacent tissues (Fig. 1A). To investigate the functional role of TRAP1 in colon cancer, we utilized the CRISPR-Cas9 system to deplete TRAP1 expression in CT26 colon cancer cell line. Successful depletion of TRAP1 was validated through western blotting across various TRAP1-deficient clones (Fig. 1B). Notably, TRAP1 protein was undetectable in these depleted cells (designated as KO lines), while the TRAP1 mRNA level remained unchanged (Fig. 1C). We then assessed the impact of TRAP1 depletion on cell proliferation by measuring cell growth for 24–72 h. As shown in Fig. 1D, TRAP1 depletion led to a

concomitant reduction in cell growth. At 72 h, cell numbers decreased significantly by over three folds in all three KO lines compared to WT cells (Fig. S1A and S1B).

To gain a comprehensive understanding of the molecular alterations induced by TRAP1 depletion, we performed proteomic analysis on cell lysates from WT and KO cells. The enrichment analysis of proteomic data using Gene Ontology (GO) Biological Process (BP) revealed downregulation of proteins involved in mitotic cell cycle, cytoplasmic translation, ribosome biogenesis, mitochondrial electron transport and NADH dehydrogenase complex assembly (mitochondrial complex I) in KO cells (Fig. 1Eand Fig. S1C, S2A, S2B). On the other hand, proteins involved in detoxification and cellular oxidant detoxification were upregulated in KO cells (Fig. 1F). Taking a closer look at mitochondrial complex I, which the enrichment analysis revealed to be downregulated in the KO cells, we observed significant reductions in several subunits—NDUFC2, NDUFS2, NDUFA10, NDUFS1 and NDUFV1—in KO cells as compared to WT (Fig. S2C). In addition, we validated the expression levels of NDUFS2 and NDUFA10 using specific antibodies in Western blot and found that these two proteins are significantly decreased in TRAP1 KO cells compared to WT cells (Fig. S2D). To confirm the potential role of TRAP1 in regulating the expression mitochondrial complex I, we analyzed the correlation between TRAP1 and mitochondrial complex I in human colon cancer samples from the TCGA database. Interestingly, we found a strong positive correlation between TRAP1 and several mitochondrial complex I subunits (Fig. S2E).

Mitochondria, the cellular powerhouses, rely on a series of complexes to efficiently generate energy. When mitochondrial complex I malfunction, it disrupts the flow of electrons, leading to the unwanted production of harmful reactive oxygen species (ROS) [59]. Therefore, we investigated the impact of TRAP1 depletion on redox homeostasis and measured intracellular ROS levels in colon cancer cells. Remarkably, TRAP1 depletion induced a dramatic 3- to 5-fold increase in ROS level (Fig. 1G and H). Restoring TRAP1 expression in KO cells (designated as KO TOE) reduced ROS level by ~60 % compared to KO cells (Fig. 1I–K), confirming the surge of ROS in KO cells was due to TRAP1 depletion. Additionally, cell cycle analysis revealed a striking shift in the cell cycle distribution of KO cells. The G0/G1 phase, indicative of cellular quiescence, was increased to >50 % in KO cells, compared to approximately 40 % in WT cells. Conversely, the S and G2/M phases, associated with DNA replication and mitosis, respectively, exhibited moderate decline in KO cells (Fig. 1L). Furthermore, the colony-forming ability of KO cells diminished by around 50 % (Fig. 1M and N). These compelling results indicate that TRAP1 depletion triggers a cascade of events, resulting in reduced cell proliferation, downregulation of mitochondrial complex I, elevated ROS generation, and cell cycle arrest in G0/G1 phase.

3.2. TRAP1 modulates metabolic switch between mitochondrial bioenergetics and glycolysis bioenergetics

Oxidative stress plays a crucial role in regulating cancer cell metabolic activity by influencing metabolic pathways to maintain redox balance. Given that TRAP1 depletion leads to excessive ROS generation, we investigated how such consequential oxidative stress may affect the metabolic profile of KO cancer cells. Intriguingly, we observed that the

culture media of KO cells became more acidic compared to the WT group (Fig. 2A). This observation prompted us to investigate the potential role of TRAP1 in cellular pH homeostasis. Direct pH measurements confirmed a significantly lower pH value in the KO cells compared to the WT cells (Fig. 2B). These findings suggest that TRAP1 depletion disrupts intracellular pH regulation, which may potentially contribute to the acidified culture media observed in KO cells.

To further elucidate the mechanism underlying the potential metabolic shift, we investigated the proteins associated with cellular pH regulation in the enrichment analysis of proteomic data of the WT and KO cells. The GSEA analysis revealed positive enrichment of two biological processes resulting from TRAP1 depletion: regulation of pH and intracellular pH reduction (Fig. 2C). Several pH regulation-related proteins were upregulated in KO cells compared to WT cells (Fig. 2D). GSEA analysis of cellular component (CC) using the proteomic data further revealed that TRAP1 depletion downregulated the proteins associated with mitochondrial and ribosomal compartments, including NADH dehydrogenase complex (complex I) and ribosomal subunit (Fig. 2E and F). These results suggest that depletion of TRAP1 may lead to mitochondrial dysfunction and metabolic alterations.

To assess the impact of TRAP1 depletion on metabolic flux, we conducted Seahorse metabolic flux analysis to evaluate mitochondrial respiration and glycolytic function. Surprisingly, the seahorse analyses revealed a remarkable tolerance of KO cells to OXPHO inhibitors (FCCP, oligomycin, rotenone) treatment (Fig. 2G), indicating reduced reliance on mitochondrial OXPHOS for energy production. Conversely, extracellular acidification rate (ECAR) measurements demonstrated a significant enhancement of glycolytic bioenergetics in KO cells, exhibiting 3- to 4-fold increases compared to WT cells (Fig. 2H). These findings were further supported by energy MAP analysis, which revealed a shift in the bioenergetic flux profile of KO cells towards glycolytic bioenergetics (Fig. 2I). To confirm the role of TRAP1 depletion in driving this metabolic shift, we directly measured glycolytic flux by assessing glucose consumption rate and lactate levels. TRAP1 depletion resulted in increased glucose consumption rate and pronounced lactate production (Fig. 2J and K), further solidifying the evidence of a metabolic switch from OXPHOS to glycolysis driven by TRAP1 depletion (Fig. 2L). These findings imply that TRAP1 plays a crucial role in regulating the metabolic balance between glycolytic bioenergetics and mitochondrial bioenergetics in colon cancer.

3.3. TRAP1 regulates mitochondrial bioenergetics through modulation of PDH activity

It has been shown that pyruvate dehydrogenase kinases (PDKs) inhibit the TCA cycle by phosphorylating PDH at serine residues 232, 293, and 300, thereby reducing PDH activity [60]. Consequently, inhibition of PDH, which normally converts pyruvate to acetyl-CoA, impedes the influx of acetyl-CoA from glycolysis into the TCA cycle [61]. Given that depletion of TRAP1 shifts metabolic bioenergetics to glycolysis and reduces mitochondrial reliance, we investigated the bioenergetic flux in KO cells by assessing PDK1 protein level and PDH phosphorylation status. As shown in Fig. 3A, KO cells exhibited significantly elevated PDK1 expression and increased PDH phosphorylation at residues S232 and S293 compared to the WT cells. Immunofluorescence staining further confirmed that PDH

phosphorylation at the S232 site was notably higher in the cytoplasm of KO cells compared to WT cells (Fig. 3B).

Further investigations using OXPHO inhibitors confirmed that KO cells were tolerant to their effects. Treatment with rotenone (complex I inhibitor) and oligomycin (complex IV inhibitor) dramatically reduced WT cell growth but had a much lesser impact on KO cells (Fig. 3C, Fig. S3A). Rotenone has been shown to cause incomplete electron transfer within cells and lead to ATP depletion and ROS production [62]. Therefore, we measured ROS levels in cells treated with either 200 nM rotenone or 200 nM oligomycin. Notably, WT cells showed a significant increase in ROS levels compared to non-treated controls, whereas KO cells remained relatively unaffected (Fig. 3D and E, Fig. S3B, S3C). Similarly, 200 nM oligomycin treatment reduced colon cancer growth and colony-forming ability in WT cells but had a much lesser extent in KO cells (Figs. S3D, S3E, S3F). These findings were further supported by assessing glycolytic flux, which revealed over a two-fold increase in glucose consumption rate and lactate acid production in 50 nM rotenone-treated WT cells compared to KO cells (Fig. 3F and G). Furthermore, immunofluorescence staining confirmed the enhanced expression of glycolysis associated proteins, GLUT1 and MCT1, in KO cells (Fig. S4A and S4B). Overall, OXPHO inhibitors significantly impact cell viability and induce metabolic reprogramming through induction of glycolytic flux in WT cells, while having minimal effects in KO cells. This difference may be attributed to the pre-existing OXPHOS defects resulting from TRAP1 depletion in KO cells. Collectively, these data suggest that TRAP1 depletion alters cellular metabolic phenotype to confer tolerance to OXPHO inhibitors by inhibiting PDH activity.

3.4. Depletion of TRAP1 renders cells more vulnerable to metabolic stress

Given that TRAP1 depletion induces mitochondrial remodeling and pushes metabolism towards glycolytic bioenergetics in colon cancer cells, we speculated that KO cells would be more susceptible to metabolic stress. To test this hypothesis, we used 2-deoxyglucose (2DG), a glucose analog that inhibits glucose consumption and ATP production [63], to investigate metabolic alterations in KO cells. As expected, KO cells showed significant reduction in colony formation and cell viability upon 2DG treatment (Fig. 3H–J, Fig. S4C). Notably, KO cells were highly sensitive even to low doses of 2DG, while WT cells remained largely unaffected by even high doses of 2DG (1.25 mM and 2.5 mM). These results indicate that depletion of TRAP1 diminishes metabolic hybrid and induces metabolic dependency in colon cancer cells. Furthermore, 2DG induced excessive ROS production specifically in KO cells, but not in WT cells (Fig. 3K and L). Additionally, 2DG treatment significantly reduced glucose consumption rate in KO cells compared to the WT cells (Fig. 3M). We also measured the cellular ADP/ATP ratio to assess how TRAP1 influenced the balance between glycolytic and oxidative metabolism under various metabolic stress conditions. Interestingly, treatment with the OXPHO inhibitor rotenone (50 nM) increased ADP/ATP ratio by ~1.5 folds in WT cells but had minimal effect in KO cells (Fig. S4D). Conversely, treatment with 2.5 mM 2DG increased ADP/ATP ratio in KO cells, but with minimal effect in WT cells (Fig. S4E). These findings suggest that TRAP1 depletion renders colon cancer cells vulnerable to 2DG-induced metabolic stress. Since 2DG induced higher ROS level in KO cells compared to WT cells, we would expect strong ER stress responses in KO cells.

Indeed, this was confirmed by elevated CHOP protein expression in KO cells. Prolonged ER stress induced by 2DG further triggered cell death and cleavage of PARP proteins in KO cells, while WT cells remained unaffected (Fig. 3N). In summary, by depleting TRAP1, we've found a way to restrict the metabolic plasticity of cancer cells and force them into a vulnerable and dependent state. This discovery makes TRAP1 a promising target for cancer therapy, providing a novel approach to combat malignant cells by targeting their metabolic plasticity.

3.5. Depletion of TRAP1 restricts metabolic plasticity to elevated glycolytic metabolism through induction of the HIF1A/HRE pathway

Next, we investigated how TRAP1 modulates the metabolic phenotype in colon cancer cells by altering the balance between glycolytic and mitochondrial bioenergetics. Our GSEA analysis of proteomic data revealed significant enrichment of several Hallmark gene sets, including hypoxia and glycolysis, in KO cells (Fig. 4A). The GSEA enrichment plots showed a positive correlation between TRAP1 depletion and the hypoxia gene set (NES: −1.74, $P < 0.005$), as well as the glycolysis gene set (NES: −1.40, $P < 0.05$) (Fig. 4B and C). Furthermore, differential gene expression analysis identified 58 upregulated and 44 downregulated genes in KO cells compared to the WT cells. The volcano plot of these differentially expressed genes is shown in Fig. 4D. Additionally, GO BP analysis highlighted significant enrichment of metabolic-associated pathways among the differentially expressed genes (Fig. 4E). Similarly, various metabolic pathways, including HIF1A signaling, and the glycolysis/gluconeogenesis pathway, were among the top 10 enriched KEGG pathways in KO cells (Fig. 4F), further supporting the notion that TRAP1 depletion in colon cancer cells triggers metabolic rewiring towards aerobic glycolysis.

To explore the potential role of HIF1A in this process, we analyzed correlation between TRAP1 and HIF1A expression, as well as between HIF1A and MCT1 expression using the TCGA colon cancer database (ENCORI). We found a strong inverse correlation between TRAP1 and HIF1A mRNA expression (correlation coefficient = −0.498, $P < 0.001$). Conversely, a positive correlation was observed between HIF1A and MCT1 expression (correlation coefficient = 0.274, $P < 0.005$) (Fig. 4G). Next, we sought to determine whether HIF1A localization plays a significant role in the observed metabolic rewiring in KO cells. Immunofluorescent staining demonstrated that HIF1A predominantly localizes to the nucleus in KO cells (Fig. 4H). These results were further confirmed by western blot analysis of subcellular fractions, including nucleus and cytoplasm (Fig. 4I), suggesting its active participation in transcriptional regulation.

We speculated that the nuclear translocation of HIF1A could activate transcription of glycolytic-associated genes in the presence of oxygen, leading to metabolic rewiring in response to oxidative stress in KO cells. In our study, the observed metabolic adaptations to enhance cancer cell survival in KO cells were likely due to the oxidative environment. To investigate this further, we employed HRE Luciferase reporter-containing cells to assess HIF1A transcriptional activity. Notably, KO cells exhibited a substantial increase (4- to 8-fold) in HRE transcriptional activation compared to WT cells (Fig. 4J). Previous studies have demonstrated that HIF1A can upregulate the expression of glycolytic flux markers such

as GLUT1 and MCT1, promoting a shift toward facultative aerobic glycolysis in cancer cells [64,65]. Following this, we examined the expression of glycolytic genes (including HIF1A, GLUT1 and MCT1) in KO cells. Western blot analysis confirmed that these markers were upregulated in KO cells compared to WT cells (Fig. 4K). Collectively, these findings support our hypothesis that TRAP1 depletion induces ROS, restricting metabolic plasticity toward a facultative glycolytic phenotype in colon cancer, potentially mediated by the HIF1A/HRE pathway (Fig. 4L).

To further confirm TRAP1 KO induced oxidative stress and shift the metabolic profile to obtain proliferation advantage, we tested additional human-derived colon cancer cell lines (HCT116, RKO, SW8, and SW480). TRAP1 inhibition led to excessive oxidative stress in 4 μM or 8 μM G-TPP-treated colon cancer cells and reduced cell viability, with various degree of responses (Fig. S5A–S5F). SW480 cells are more resistant to G-TPP treatment, whereas SW48 cells are highly sensitive. Furthermore, we observed consistent suppression of PDH activity in all four cell lines, along with HIF1A activation in HCT116 and RKO cells (Fig. S5G–S5H). These findings are consistent with the observations in CT-26 cells, reinforcing the conclusion that TRAP1 knockout induces oxidative stress and promotes a metabolic shift toward glycolysis.

3.6. Restoring TRAP1 permits metabolic plasticity and protects cancer cells from the glycolytic inhibitor treatment

After revealing that TRAP1 depletion in colon cancer cells restricts metabolic plasticity by inhibiting PDH activity, we proceeded to restore TRAP1 expression in KO cells to investigate if reintroducing TRAP1 in KO cells could at least partially reverse the effects caused by its depletion. As expected, re-introduction of TRAP1 in KO cells led to a significant reduction in PDK1 expression and PDH phosphorylation (Fig. 5A and B). This TRAP1 restoration not only restored mitochondrial PDH activity but also re-sensitized the cells to rotenone treatment to a degree similar to WT cells (Fig. 5C). Furthermore, TRAP1-restored KO cells exhibited elevated intracellular ROS levels upon rotenone treatment compared to non-treatment controls, whereas KO cells were relatively resistant to rotenone (Fig. 5D and E). These data suggest that restoring TRAP1 expression reverses the metabolic reprogramming observed in KO cells, validating our phenotypic and molecular observations in KO wells as TRAP1-dependent.

Furthermore, restoring TRAP1 expression reduced HIF1A nuclear localization (Fig. 5F), and significantly downregulated the expression of HIF1A downstream genes, including GLUT1 and MCT1 (Fig. 5G, Fig. S6A and S6B). Restoration of TRAP1 also led to reduction in extracellular acidification and glycolytic flux in the cells (Fig. S6C and S6D). Consequently, lactate acid production and glucose consumption rate were also corrected to levels similar or closer to WT cells (Fig. 5H and I). Additionally, restoring TRAP1 alleviated oxidative stress induced by 2DG treatment in the cancer cells (Fig. 5J and K). In essence, restoring TRAP1 in KO cells recovers the cells to a metabolic hybrid state, enabling metabolic plasticity. This explains why restoring TRAP1 protected the cancer cells from the glycolytic inhibitor 2DG treatment (Fig. 5L). Collectively, these findings demonstrate that

TRAP1 acts as a switch, controlling the metabolic phenotype of cancer cells by permitting or restricting metabolic plasticity.

3.7. ROS detoxification alleviates the activation of HIF1A/HRE axis in KO cells

Previous studies have demonstrated that intracellular ROS can stabilize HIF1A and activate the glycolysis pathway in cancer cells [66,67]. To elucidate the roles of ROS in the context of HIF1A activation and TRAP1 depletion under oxygen-rich conditions, we used ROS scavenger Trolox to treat the WT and KO cells. After 2 h of treatment, 2 mM Trolox significantly reduced the intracellular ROS induced by TRAP1 depletion (Fig. 6A and B). Furthermore, HIF1A nuclear localization was greatly diminished in 1 mM Trolox-treated KO cells compared to non-Trolox control KO cells. In comparison, Trolox treatment only slightly reduced HIF1A nuclear localization in WT ells (Fig. 6C). These results further strengthen the link between ROS and HIF1A activation in this specific context.

Next, we conducted a reporter assay to directly assess the impact of ROS detoxification on the transcriptional activation of HRE in KO cells. As shown in Fig. 6D, the luminescence from the HRE reporter was significantly reduced in the Trolox treatment groups compared to the non-treatment groups in KO cells, while the WT cells were not affected by the Trolox treatment. Notably, by restoring redox homeostasis through ROS scavenging with Trolox, we observed downregulation of aerobic glycolysis-associated genes, including HIF1A, GLUT1, and MCT1 in KO cells (Fig. 6E). Furthermore, the pH of the culture medium increased in Trolox-treated KO cells compared to the control groups, in a dosage-dependent (Fig. 6F). To explore the impact of Trolox on glycolytic flux in KO cells, we investigated its effects on lactic acid levels and glucose consumption. Interestingly, Trolox treatment led to decreased glucose consumption in the KO2 and KO7 clones, while lactic acid levels was reduced across all three KO clones (Fig. 6G and H). These results further underscore the crucial role of ROS in HIF1A/HRE pathway activation and subsequent metabolic reprogramming in KO cancer cells.

To further elucidate how TRAP1 depletion modulates metabolic rewiring through HIF1A signaling, we employed the HIF1A inhibitor PX-478 to inactivate HIF1A in KO cells. As shown in Fig. 6I, this treatment led to significant reduction in HIF1A protein level, accompanied by downregulation of its downstream targets, GLUT1 and MCT1. Consequently, glycolytic flux was diminished (Fig. 6J and K). To further explore the role of HIF1A in regulating mitochondrial bioenergetics, we examined its impact on the PDK1/PDH axis. Inhibition of HIF1A using PX-478 decreased PDK1 expression and restored PDH activity through reduction of phosphorylation at PDH(S232) in clone 2 and clone 7, but not in clone 6 (Fig. 6L and M). These results suggest that cancer cells lacking TRAP1 ramp up their production of harmful ROS, which in turn activates HIF1A — a pivotal player in energy production. HIF1A not only promotes aerobic glycolysis through upregulation of glycolysis enzymes, but also activates PDKs to reduce PDH activities, further suppressing the mitochondrial bioenergetics. These bioenergetic shifts redirect cells away from efficient mitochondrial power generation and towards a less efficient process (aerobic glycolysis).

3.8. Restoration of PDH activity exacerbates oxidative stress and cell death in KO cells

PDKs phosphorylate PDH, inhibiting its activity and thereby preventing the conversion of pyruvate to acetyl-CoA and shifting the cellular metabolic profile away from OXPHO. Depletion of TRAP1 led to upregulation of PDKs in all three KO clones (Fig. S7A). Dichloroacetic acid (DCA), a known PDKs inhibitor, activates PDH activity and has been shown to restore oxidative phosphorylation in colon cancer [25]. To evaluate the forced activation of PDH in the context of TRAP1 depletion, we treated KO cells with 20 mM DCA to restore PDH activity and analyzed the metabolic profile and cell viability. As expected, DCA-treated KO cells showed a significant decrease in both PDK1 protein expression and PDH phosphorylation at serine residues 232 and 293 (Fig. 7A and B).

Next, we assessed the glycolytic flux in DCA-treated cells by measuring the pH of the culture media. The pH values of the culture media in DCA-treated KO cells were significantly higher compared to untreated controls (Fig. 7C and D). Furthermore, we characterized the glycolytic flux by measuring glucose consumption rate and lactic acid level in DCA-treated cells. Both measurements were significantly reduced in DCA-treated KO cells, reaching levels similar to those in WT cells (Fig. 7E and F). These results suggest that DCA suppresses the aerobic glycolysis pathway and shifts the glycolytic bioenergetics towards mitochondria bioenergetics in KO cells. Since TRAP1 depletion led to a substantial increase in ROS, we speculated that treatment with DCA (which activates PDH) might further elevate ROS levels in KO cells. Indeed, we observed a dramatic rise in ROS levels specifically in DCA-treated KO cells, with a much lesser increase in WT cells (Fig. 7G and H). Additionally, TRAP1-restored KO cells displayed ROS generation patterns more similar to WT cells than KO cells when treated with DCA (Fig. S7B and S7C). Beyond the increase of ROS levels, DCA treatment and TRAP1 depletion synergistically suppressed cell viability and colony formation in KO cells, with fewer effects observed in WT cells (Fig. 7I–K, Fig. S7D). These results suggest that DCA disrupted the cellular ROS detoxification capacity by shifting the metabolic pathway towards the OXPHO pathway in mitochondrial dysfunction cells (KO cells).

It has been reported that DCA can restore chemosensitivity to 5-FU in colon cancer by modulating glycolysis [68]. Recent studies also suggest that targeting OXPHOS could be an emerging strategy in cancer therapy to reduce drug resistance [69]. In this study, we observed that DCA enhanced the efficacy of OXPHOS inhibitors in TRAP1 KO cells compared to treatment with OXPHOS inhibitors alone. In contrast, OXPHOS inhibitors increased the efficacy of DCA in WT cells compared to DCA alone. These findings indicate that TRAP1 KO cells exhibit a distinct metabolic profile characterized by mitochondrial dysfunction. As shown in Fig. S7E–S7F, DCA treatment restored the sensitivity of KO cells to OXPHOS inhibition, thereby suppressing cancer cell growth. Collectively, these results suggest that TRAP1 depletion impairs PDH activity, leading to reduced mitochondrial energetics and making cells more reliant on glycolysis for survival. Further modulation of glycolysis through DCA treatment leads to a dramatic increase in ROS, resulting in significant decrease in cell proliferation and increase of cell death (Fig. 7L). Combining TRAP1 inhibition with DCA treatment exhibits a synergistic suppressive effect on colon cancer.

4. Discussion

Cancer cells often exploit metabolic plasticity to adapt to their metabolism, enabling survival under the stress conditions encountered during tumor development, metastasis, and cancer therapy [9,70,71]. Metabolic plasticity empowers cancer cells to adapt to oxidative stress through two main strategies: 1) Upregulating their antioxidant capacity to directly detoxify ROS, and 2) Rewiring their metabolic bioenergetics to mitigate ROS production [72]. The mitochondrial protein TRAP1 has been implicated in various cellular processes, including the regulation of metabolic energy, ROS detoxification, and cell survival [37]. In this study, we employed CRISPR/Cas9 mediated genetic deletion to knock out TRAP1 in colon cancer cells to investigate the roles of TRAP1 in regulating tumor cell metabolism and survival. We found that KO cells exhibited excessive ROS generation and reduced cell proliferation. Intriguingly, these KO cells undertook metabolic reprogramming to adapt to oxidative conditions to enhance their survival. This metabolic reprogramming in KO cells involved a restriction of mitochondrial bioenergetics and a shift towards glycolytic bioenergetics. Our study provides new insights into how TRAP1 depletion influences metabolic plasticity, enabling colon cancer cells to adapt to metabolic and oxidative stress.

Our previous study demonstrated that inhibiting TRAP1 led to activation of NRF2, the master regulator of the antioxidant response. Combining an NRF2 inhibitor with a TRAP1 inhibitor resulted in excessive ROS levels surpassing the cytotoxic threshold, thereby exacerbating cell death [49]. TRAP1 has been shown to influence the balance between oxidative phosphorylation and glycolysis, potentially rewiring cellular metabolism [50]. Additionally, TRAP1 appears to regulate mitochondrial activity through interactions with complex III [73]. While studies have suggested that TRAP1 inhibition leads to a metabolic switch towards glycolysis, the precise role of TRAP1 in favoring either oxidative phosphorylation or glycolysis remains controversial and requires further investigation. In our current study, we observed significantly decreased expression of mitochondrial complex I subunits (NDUFC2, NDUFS2, NDUFA10, NDUFS1, NDUFV1, and NDUFS4) in KO cells. In addition, KO cells exhibited resistance to rotenone (a complex I inhibitor) and oligomycin (a complex IV inhibitor), indicating diminished mitochondrial reliance. These results clearly demonstrate that TRAP1 is involved in the regulation of mitochondrial function through mitochondrial complex I. Furthermore, we found that TRAP1 depletion not only impaired mitochondrial bioenergetics but also increased glucose uptake and lactate secretion, rendering the cells sensitive to inhibition of glycolysis. These findings indicate that TRAP1 depletion limits the metabolic plasticity of colon cancer cells, forcing them towards increased glycolytic state and making them dependent on this pathway for survival.

Cell metabolic plasticity is governed by master regulators AMPK and HIF1A, which control cellular energy homeostasis and aerobic glycolysis, respectively [74]. These two master regulator genes enable cancer cells to stay in a hybrid metabolic phenotype, efficiently producing energy through various metabolism pathways [70]. This hybrid metabolic phenotype not only keeps ROS at moderate and balanced levels, benefiting cancer cell signaling, but also prevents DNA damage due to excessive ROS [75,76]. In this study, proteomics analysis revealed that glycolysis gene set and HIF1A signaling pathway were significantly enriched in KO cells. These results were further validated through HIF1A

nuclear localization (immunofluorescence staining) and induction of highly transcriptional activation of hypoxia response elements (reporter assay). HIF1A stimulates the expression of glycolysis-associated genes and represses mitochondrial function by inducing PDK1 under hypoxic conditions [24,77]. Consequently, HIF1A downstream genes, including GLUT1 and MCT1, were significantly upregulated, and glycolytic flux was dramatically enhanced in KO cells. Consistent with these findings, ROS scavenger Trolox reversed glycolytic flux and HIF1A activation in KO cells. Furthermore, restoration of TRAP1 expression in KO cells decreased HIF1A, GLUT1, MCT1, pPDH (S232), and ROS generation, reversing the metabolic reprogramming effects observed in KO cells. These findings suggest that TRAP1 depletion induces ROS generation, leading to activation of the HIF1A pathway and a preference for aerobic glycolysis in colon cancer cells.

Our findings further reveal that TRAP1 depletion not only induces a metabolic shift towards glycolysis for ROS detoxification via the HIF1A pathway but also restricts mitochondrial bioenergetics by suppressing PDH activity. Furthermore, inhibiting HIF1A with PX-478 decreased GLUT1 and MCT1 expression, and restored PDH activity in KO cells. Collectively, these results suggest that TRAP1 tailors the metabolic phenotype of colon cancer cells by regulating the ROS/HIF1A/PDH axis to adapt stressful conditions. These novel findings support TRAP1 as a potential therapeutic target for modulating cancer metabolism and impeding tumor progression. Previous research suggests that targeting metabolic plasticity through combination therapies holds promise for colon cancer treatment, potentially improving patient outcomes [78]. An earlier study demonstrated that targeting metabolic plasticity with mitochondrial HSP90 inhibitor induced mitochondrial dysfunction and enhanced the efficacy of MAPK inhibitor treatment in cancer cells [12]. Our study aligns with this concept, as our data suggests that TRAP1 depletion enhances metabolic dependence in colon cancer cells, making them more susceptible to therapeutic intervention. Notably, the PDK inhibitor DCA, a current clinical drug used for lactic acidosis in mitochondrial defects [79,80], specifically increased mitochondrial dependence and augmented the cytotoxic effects in KO cells, but not in WT cells. Remarkably, combining DCA or 2DG with TRAP1 depletion exhibited synergistic suppressive effects, suggesting a potential therapeutic strategy.

In conclusion, our study demonstrates that TRAP1 modulates metabolic switch between mitochondrial bioenergetics and glycolytic bioenergetics. Depletion of TRAP1 induces metabolic shift towards glycolysis in colon cancer cells, enabling them to adapt to oxidative stress and ensure survival. Consequently, depletion of TRAP1 creates a metabolic vulnerability as well as metabolic dependency on glycolysis, presenting a potential therapeutic strategy for colon cancer. This opens an exciting new path for developing novel therapies targeting cancer metabolism.

Supplementary Material

Refer to Web version on PubMed Central for supplementary material.

Acknowledgements

We thank the laboratory of Dr. Yong Li for technical assistance. This work was funded by NIH/NCI grant R01CA211892 and R01CA276173 and supported in part by the Texas Medical Center Digestive Disease Center (P30DK056338).

Data statement

All data in this study are included in this article and the supplementary files.

Appendix A. Supplementary data

Supplementary data to this article can be found online at https://doi.org/10.1016/j.canlet.2025.217977.

Abbreviations:

KO	knockout
TRAP1 EV	TRAP1 empty vector
TRAP1 OE	TRAP1 overexpression
HREs	hypoxia response elements
ROS	reactive oxygen species
OXPHOS	oxidative phosphorylation
TCA	tricarboxylic acid
PDK1	pyruvate dehydrogenase kinases 1
PDH	pyruvate dehydrogenase
DCA	dichloroacetic acid
Ctrl	control

References

[1]. Bray F, Ferlay J, Soerjomataram I, Siegel RL, Torre LA, Jemal A, Global cancer statistics 2018: GLOBOCAN estimates of incidence and mortality worldwide for 36 cancers in 185 countries, CA Cancer J. Clin. 68 (2018) 394–424. [PubMed: 30207593]

[2]. Pang B, Wu H, Metabolic reprogramming in colorectal cancer: a review of aerobic glycolysis and its therapeutic implications for targeted treatment strategies, Cell Death Discov. 11 (2025) 321. [PubMed: 40659604]

[3]. Qin R, Fan X, Huang Y, Chen S, Ding R, Yao Y, Wu R, Duan Y, Li X, Khan HU, Hu J, Wang H, Role of glucose metabolic reprogramming in colorectal cancer progression and drug resistance, Transl. Oncol. 50 (2024) 102156. [PubMed: 39405607]

[4]. Faubert B, Solmonson A, DeBerardinis RJ, Metabolic reprogramming and cancer progression, Science 368 (2020).

[5]. Yang J, Shay C, Saba NF, Teng Y, Cancer metabolism and carcinogenesis, Exp. Hematol. Oncol. 13 (2024) 10. [PubMed: 38287402]

[6]. Rahman M, Hasan MR, Cancer metabolism and drug resistance, Metabolites 5 (2015) 571–600. [PubMed: 26437434]

[7]. Flora GD, Nayak MK, Ghatge M, Kumskova M, Patel RB, Chauhan AK, Mitochondrial pyruvate dehydrogenase kinases contribute to platelet function and thrombosis in mice by regulating aerobic glycolysis, Blood Adv. 7 (2023) 2347–2359. [PubMed: 36971790]

[8]. Dupuy F, Tabaries S, Andrzejewski S, Dong Z, Blagih J, Annis MG, Omeroglu A, Gao D, Leung S, Amir E, Clemons M, Aguilar-Mahecha A, Basik M, Vincent EE, St-Pierre J, Jones RG, Siegel PM, PDK1-Dependent metabolic reprogramming dictates metastatic potential in breast cancer, Cell Metab. 22 (2015) 577–589. [PubMed: 26365179]

[9]. McGuirk S, Audet-Delage Y, St-Pierre J, Metabolic fitness and plasticity in cancer progression, Trends Cancer 6 (2020) 49–61. [PubMed: 31952781]

[10]. Nuyttens L, Vandewalle J, Libert C, Sepsis-induced changes in pyruvate metabolism: insights and potential therapeutic approaches, EMBO Mol. Med. 16 (2024) 2678–2698. [PubMed: 39468303]

[11]. Genini D, Brambilla L, Laurini E, Merulla J, Civenni G, Pandit S, D'Antuono R, Perez L, Levy DE, Pricl S, Carbone GM, Catapano CV, Mitochondrial dysfunction induced by a SH2 domain-targeting STAT3 inhibitor leads to metabolic synthetic lethality in cancer cells, Proc. Natl. Acad. Sci. U. S. A. 114 (2017) E4924–E4933. [PubMed: 28584133]

[12]. Zhang G, Frederick DT, Wu L, Wei Z, Krepler C, Srinivasan S, Chae YC, Xu X, Choi H, Dimwamwa E, Ope O, Shannan B, Basu D, Zhang D, Guha M, Xiao M, Randell S, Sproesser K, Xu W, Liu J, Karakousis GC, Schuchter LM, Gangadhar TC, Amaravadi RK, Gu M, Xu C, Ghosh A, Xu W, Tian T, Zhang J, Zha S, Liu Q, Brafford P, Weeraratna A, Davies MA, Wargo JA, Avadhani NG, Lu Y, Mills GB, Altieri DC, Flaherty KT, Herlyn M, Targeting mitochondrial biogenesis to overcome drug resistance to MAPK inhibitors, J. Clin. Investig. 126 (2016) 1834–1856. [PubMed: 27043285]

[13]. Mathew M, Nguyen NT, Bhutia YD, Sivaprakasam S, Ganapathy V, Metabolic signature of warburg effect in cancer: an effective and obligatory interplay between nutrient transporters and catabolic/anabolic pathways to promote tumor growth, Cancers (Basel) 16 (2024).

[14]. Warburg O, On the origin of cancer cells, Science 123 (1956) 309–314. [PubMed: 13298683]

[15]. Warburg O, Wind F, Negelein E, The metabolism of tumors in the body, J. Gen. Physiol. 8 (1927) 519–530. [PubMed: 19872213]

[16]. Tonks NK, Redox redux: revisiting PTPs and the control of cell signaling, Cell 121 (2005) 667–670. [PubMed: 15935753]

[17]. Yang M, Haase AD, Huang FK, Coulis G, Rivera KD, Dickinson BC, Chang CJ, Pappin DJ, Neubert TA, Hannon GJ, Boivin B, Tonks NK, Dephosphorylation of tyrosine 393 in argonaute 2 by protein tyrosine phosphatase 1B regulates gene silencing in oncogenic RAS-Induced senescence, Mol. Cell 55 (2014) 782–790. [PubMed: 25175024]

[18]. Bae T, Hallis SP, Kwak MK, Hypoxia, oxidative stress, and the interplay of HIFs and NRF2 signaling in cancer, Exp. Mol. Med. 56 (2024) 501–514. [PubMed: 38424190]

[19]. Tello D, Balsa E, Acosta-Iborra B, Fuertes-Yebra E, Elorza A, Ordonez A, Corral-Escariz M, Soro I, Lopez-Bernardo E, Perales-Clemente E, Martinez-Ruiz A, Enriquez JA, Aragones J, Cadenas S, Landazuri MO, Induction of the mitochondrial NDUFA4L2 protein by HIF-1alpha decreases oxygen consumption by inhibiting complex I activity, Cell Metab. 14 (2011) 768–779. [PubMed: 22100406]

[20]. Zhang J, Yao M, Xia S, Zeng F, Liu Q, Systematic and comprehensive insights into HIF-1 stabilization under normoxic conditions: implications for cellular adaptation and therapeutic strategies in cancer, Cell. Mol. Biol. Lett. 30 (2025) 2. [PubMed: 39757165]

[21]. Levine AJ, Puzio-Kuter AM, The control of the metabolic switch in cancers by oncogenes and tumor suppressor genes, Science 330 (2010) 1340–1344. [PubMed: 21127244]

[22]. Nsiah NY, Morgan AB, Donkor N, Inman DM, Long-term HIF-1alpha stabilization reduces respiration, promotes mitophagy, and results in retinal cell death, Sci. Rep. 13 (2023) 20541. [PubMed: 37996657]

[23]. Holness MJ, Sugden MC, Regulation of pyruvate dehydrogenase complex activity by reversible phosphorylation, Biochem. Soc. Trans. 31 (2003) 1143–1151. [PubMed: 14641014]

[24]. Kim JW, Tchernyshyov I, Semenza GL, Dang CV, HIF-1-mediated expression of pyruvate dehydrogenase kinase: a metabolic switch required for cellular adaptation to hypoxia, Cell Metab. 3 (2006) 177–185. [PubMed: 16517405]

[25]. Madhok BM, Yeluri S, Perry SL, Hughes TA, Jayne DG, Dichloroacetate induces apoptosis and cell-cycle arrest in colorectal cancer cells, Br. J. Cancer 102 (2010) 1746–1752. [PubMed: 20485289]

[26]. Avolio R, Agliarulo I, Criscuolo D, Sarnataro D, Auriemma M, De Lella S, Pennacchio S, Calice G, Ng MY, Giorgi C, Pinton P, Cooperman BS, Landriscina M, Esposito F, Matassa DS, Cytosolic and mitochondrial translation elongation are coordinated through the molecular chaperone TRAP1 for the synthesis and import of mitochondrial proteins, Genome Res. 33 (2023) 1242–1257. [PubMed: 37487647]

[27]. Kang BH, Plescia J, Dohi T, Rosa J, Doxsey SJ, Altieri DC, Regulation of tumor cell mitochondrial homeostasis by an organelle-specific Hsp90 chaperone network, Cell 131 (2007) 257–270. [PubMed: 17956728]

[28]. Kim SY, Yoon NG, Im JY, Lee JH, Kim J, Jeon Y, Choi YJ, Lee JH, Uemura A, Park DH, Kang BH, Targeting the mitochondrial chaperone TRAP1 alleviates vascular pathologies in ischemic retinopathy, Adv. Sci. (Weinh.) 11 (2024) e2302776. [PubMed: 37983591]

[29]. Bruno G, Pietrafesa M, Crispo F, Piscazzi A, Maddalena F, Giordano G, Conteduca V, Garofoli M, Porras A, Esposito F, Landriscina M, TRAP1 modulates mitochondrial biogenesis via PGC-1alpha/TFAM signalling pathway in colorectal cancer cells, J. Mol. Med. (Berl.) 102 (2024) 1285–1296. [PubMed: 39210159]

[30]. Saleem MZ, Huang R, Huang Y, Guo X, Liu Y, Gao M, Fan Y, Chen ZS, Ke ZF, Ye S, Xu J, Targeting TRAP1-dependent metabolic reprogramming to overcome doxorubicin resistance in quiescent breast cancer, Drug Resist. Updates 81 (2025) 101226.

[31]. Leav I, Plescia J, Goel HL, Li J, Jiang Z, Cohen RJ, Languino LR, Altieri DC, Cytoprotective mitochondrial chaperone TRAP-1 as a novel molecular target in localized and metastatic prostate cancer, Am. J. Pathol. 176 (2010) 393–401. [PubMed: 19948822]

[32]. Siegelin MD, Plescia J, Raskett CM, Gilbert CA, Ross AH, Altieri DC, Global targeting of subcellular heat shock protein-90 networks for therapy of glioblastoma, Mol. Cancer Therapeut. 9 (2010) 1638–1646.

[33]. Dharaskar SP, Paithankar K, Amere Subbarao S, Analysis and functional relevance of the chaperone TRAP-1 interactome in the metabolic regulation and mitochondrial integrity of cancer cells, Sci. Rep. 13 (2023) 7584. [PubMed: 37165028]

[34]. Amoroso MR, Matassa DS, Agliarulo I, Avolio R, Lu H, Sisinni L, Lettini G, Gabra H, Landriscina M, Esposito F, TRAP1 downregulation in human ovarian cancer enhances invasion and epithelial-mesenchymal transition, Cell Death Dis. 7 (2016) e2522. [PubMed: 27977010]

[35]. Laquatra C, Magro A, Guarra F, Lambrughi M, Ferrone L, Fracasso G, Bacchin M, La Spina M, Moroni E, Papaleo E, Colombo G, Rasola A, Point mutations of the mitochondrial chaperone TRAP1 affect its functions and pro-neoplastic activity, Cell Death Dis. 16 (2025) 172. [PubMed: 40074754]

[36]. Liu F, Lin X, Wu X, Sui X, Ren W, Wang Q, Wang Y, Luo Y, Cao J, The role of TRAP1 in regulating mitochondrial dynamics during acute hypoxia-induced brain injury, J. Transl. Med. 22 (2024) 974. [PubMed: 39468583]

[37]. Dharaskar SP, Amere Subbarao S, The mitochondrial chaperone TRAP-1 regulates the glutamine metabolism in tumor cells, Mitochondrion 69 (2023) 159–170. [PubMed: 36828164]

[38]. Chen R, Lai LA, Brentnall TA, Pan S, Biomarkers for colitis-associated colorectal cancer, World J. Gastroenterol. 22 (2016) 7882–7891. [PubMed: 27672285]

[39]. Chen R, Pan S, Lai K, Lai LA, Crispin DA, Bronner MP, Brentnall TA, Up-regulation of mitochondrial chaperone TRAP1 in ulcerative colitis associated colorectal cancer, World J. Gastroenterol. 20 (2014) 17037–17048. [PubMed: 25493016]

[40]. May D, Pan S, Crispin DA, Lai K, Bronner MP, Hogan J, Hockenbery DM, McIntosh M, Brentnall TA, Chen R, Investigating neoplastic progression of ulcerative colitis with label-free comparative proteomics, J. Proteome Res. 10 (2011) 200–209. [PubMed: 20828217]

[41]. Merfeld T, Peng S, Keegan BM, Crowley VM, Brackett CM, Gutierrez A, McCann NR, Reynolds TS, Rhodes MC, Byrd KM, Deng J, Matts RL, Blagg BSJ, Elucidation of novel TRAP1-Selective inhibitors that regulate mitochondrial processes, Eur. J. Med. Chem. 258 (2023) 115531. [PubMed: 37307624]

[42]. Kang BH, Plescia J, Song HY, Meli M, Colombo G, Beebe K, Scroggins B, Neckers L, Altieri DC, Combinatorial drug design targeting multiple cancer signaling networks controlled by mitochondrial Hsp90, J. Clin. Investig. 119 (2009) 454–464. [PubMed: 19229106]

[43]. Kang BH, Siegelin MD, Plescia J, Raskett CM, Garlick DS, Dohi T, Lian JB, Stein GS, Languino LR, Altieri DC, Preclinical characterization of mitochondria-targeted small molecule hsp90 inhibitors, gamitrinibs, in advanced prostate cancer, Clin. Cancer Res. 16 (2010) 4779–4788. [PubMed: 20876793]

[44]. Nguyen TTT, Ishida CT, Shang E, Shu C, Bianchetti E, Karpel-Massler G, Siegelin MD, Activation of LXR receptors and inhibition of TRAP1 causes synthetic lethality in solid tumors, Cancers (Basel) 11 (2019).

[45]. Karpel-Massler G, Ishida CT, Bianchetti E, Shu C, Perez-Lorenzo R, Horst B, Banu M, Roth KA, Bruce JN, Canoll P, Altieri DC, Siegelin MD, Inhibition of mitochondrial matrix chaperones and antiapoptotic Bcl-2 family proteins empower antitumor therapeutic responses, Cancer Res. 77 (2017) 3513–3526. [PubMed: 28522750]

[46]. Sawai A, Chandarlapaty S, Greulich H, Gonen M, Ye Q, Arteaga CL, Sellers W, Rosen N, Solit DB, Inhibition of Hsp90 down-regulates mutant epidermal growth factor receptor (EGFR) expression and sensitizes EGFR mutant tumors to paclitaxel, Cancer Res. 68 (2008) 589–596. [PubMed: 18199556]

[47]. Landriscina M, Laudiero G, Maddalena F, Amoroso MR, Piscazzi A, Cozzolino F, Monti M, Garbi C, Fersini A, Pucci P, Esposito F, Mitochondrial chaperone Trap1 and the calcium binding protein sorcin interact and protect cells against apoptosis induced by antiblastic agents, Cancer Res. 70 (2010) 6577–6586. [PubMed: 20647321]

[48]. Wang N, Zhu P, Huang R, Sun L, Dong D, Gao Y, Suppressing TRAP1 sensitizes glioblastoma multiforme cells to temozolomide, Exp. Ther. Med. 22 (2021) 1246. [PubMed: 34539842]

[49]. Tsai HY, Bronner MP, March JK, Valentine JF, Shroyer NF, Lai LA, Brentnall TA, Pan S, Chen R, Metabolic targeting of NRF2 potentiates the efficacy of the TRAP1 inhibitor G-TPP through reduction of ROS detoxification in colorectal cancer, Cancer Lett. 549 (2022) 215915. [PubMed: 36113636]

[50]. Yoshida S, Tsutsumi S, Muhlebach G, Sourbier C, Lee MJ, Lee S, Vartholomaiou E, Tatokoro M, Beebe K, Miyajima N, Mohney RP, Chen Y, Hasumi H, Xu W, Fukushima H, Nakamura K, Koga F, Kihara K, Trepel J, Picard D, Neckers L, Molecular chaperone TRAP1 regulates a metabolic switch between mitochondrial respiration and aerobic glycolysis, Proc. Natl. Acad. Sci. U. S. A. 110 (2013) E1604–E1612. [PubMed: 23564345]

[51]. Rasola A, Neckers L, Picard D, Mitochondrial oxidative phosphorylation TRAP(1) ped in tumor cells, Trends Cell Biol. 24 (2014) 455–463. [PubMed: 24731398]

[52]. Sciacovelli M, Guzzo G, Morello V, Frezza C, Zheng L, Nannini N, Calabrese F, Laudiero G, Esposito F, Landriscina M, Defilippi P, Bernardi P, Rasola A, The mitochondrial chaperone TRAP1 promotes neoplastic growth by inhibiting succinate dehydrogenase, Cell Metab. 17 (2013) 988–999. [PubMed: 23747254]

[53]. Laquatra C, Sanchez-Martin C, Dinarello A, Cannino G, Minervini G, Moroni E, Schiavone M, Tosatto S, Argenton F, Colombo G, Bernardi P, Masgras I, Rasola A, HIF1alpha-dependent induction of the mitochondrial chaperone TRAP1 regulates bioenergetic adaptations to hypoxia, Cell Death Dis. 12 (2021) 434. [PubMed: 33934112]

[54]. Lisanti S, Tavecchio M, Chae YC, Liu Q, Brice AK, Thakur ML, Languino LR, Altieri DC, Deletion of the mitochondrial chaperone TRAP-1 uncovers global reprogramming of metabolic networks, Cell Rep. 8 (2014) 671–677. [PubMed: 25088416]

[55]. Peng H, Pan S, Yan Y, Brand RE, Petersen GM, Chari ST, Lai LA, Eng JK, Brentnall TA, Chen R, Systemic proteome alterations linked to early stage pancreatic cancer in diabetic patients, Cancers (Basel) (2020) 12.

[56]. Senavirathna L, Ma C, Chen R, Pan S, Proteomic investigation of glyceraldehyde-derived intracellular AGEs and their potential influence on pancreatic ductal cells, Cells 10 (2021).

[57]. Eng JK, Jahan TA, Hoopmann MR, Comet: an open-source MS/MS sequence database search tool, Proteomics 13 (2013) 22–24. [PubMed: 23148064]

[58]. Deutsch EW, Mendoza L, Shteynberg D, Slagel J, Sun Z, Moritz RL, Trans-proteomic pipeline, a standardized data processing pipeline for large-scale reproducible proteomics informatics, Proteonomics Clin. Appl. 9 (2015) 745–754.

[59]. Adhikary A, Mukherjee A, Banerjee R, Nagotu S, DRP1: at the crossroads of dysregulated mitochondrial dynamics and altered cell signaling in cancer cells, ACS Omega 8 (2023) 45208–45223. [PubMed: 38075775]

[60]. Woolbright BL, Rajendran G, Abbott E, Martin A, Didde R, Dennis K, Harris RA, Taylor JA 3rd, Pyruvate dehydrogenase kinase 4 deficiency increases tumorigenesis in a murine model of bladder cancer, Cancers (Basel) 15 (2023).

[61]. Arnold PK, Finley LWS, Regulation and function of the Mammalian tricarboxylic acid cycle, J. Biol. Chem. 299 (2023) 102838. [PubMed: 36581208]

[62]. Roy T, Chatterjee A, Swarnakar S, Rotenone induced neurodegeneration is mediated via cytoskeleton degradation and necroptosis, Biochim. Biophys. Acta Mol. Cell Res. 1870 (2023) 119417. [PubMed: 36581087]

[63]. Singh R, Gupta V, Kumar A, Singh K, 2-Deoxy-D-Glucose: a novel pharmacological agent for killing hypoxic tumor cells, oxygen dependence-lowering in Covid-19, and other pharmacological activities, Adv. Pharmacol. Pharm. Sci. 2023 (2023) 9993386. [PubMed: 36911357]

[64]. Miranda-Goncalves V, Granja S, Martinho O, Honavar M, Pojo M, Costa BM, Pires MM, Pinheiro C, Cordeiro M, Bebiano G, Costa P, Reis RM, Baltazar F, Hypoxia-mediated upregulation of MCT1 expression supports the glycolytic phenotype of glioblastomas, Oncotarget 7 (2016) 46335–46353. [PubMed: 27331625]

[65]. Ebert BL, Firth JD, Ratcliffe PJ, Hypoxia and mitochondrial inhibitors regulate expression of glucose transporter-1 via distinct Cis-acting sequences, J. Biol. Chem. 270 (1995) 29083–29089. [PubMed: 7493931]

[66]. Shi DY, Xie FZ, Zhai C, Stern JS, Liu Y, Liu SL, The role of cellular oxidative stress in regulating glycolysis energy metabolism in hepatoma cells, Mol. Cancer 8 (2009) 32. [PubMed: 19497135]

[67]. Fruehauf JP, Meyskens FL Jr., Reactive oxygen species: a breath of life or death? Clin. Cancer Res. 13 (2007) 789–794. [PubMed: 17289868]

[68]. Koltai T, Fliegel L, Dichloroacetate for cancer treatment: some facts and many doubts, Pharmaceuticals 17 (2024).

[69]. Ashton TM, McKenna WG, Kunz-Schughart LA, Higgins GS, Oxidative phosphorylation as an emerging target in cancer therapy, Clin. Cancer Res. 24 (2018) 2482–2490. [PubMed: 29420223]

[70]. Jia D, Lu M, Jung KH, Park JH, Yu L, Onuchic JN, Kaipparettu BA, Levine H, Elucidating cancer metabolic plasticity by coupling gene regulation with metabolic pathways, Proc. Natl. Acad. Sci. U. S. A. 116 (2019) 3909–3918. [PubMed: 30733294]

[71]. Palm W, Metabolic plasticity allows cancer cells to thrive under nutrient starvation, Proc. Natl. Acad. Sci. U. S. A. 118 (2021).

[72]. Bhardwaj V, He J, Reactive oxygen species, metabolic plasticity, and drug resistance in cancer, Int. J. Mol. Sci. 21 (2020).

[73]. Matassa DS, Criscuolo D, Avolio R, Agliarulo I, Sarnataro D, Pacelli C, Scrima R, Colamatteo A, Matarese G, Capitanio N, Landriscina M, Esposito F, Regulation of mitochondrial complex III activity and assembly by TRAP1 in cancer cells, Cancer Cell Int. 22 (2022) 402. [PubMed: 36510251]

[74]. Zhong ZT, Wang XY, Pan Y, Zhou K, Chen JH, Gao YQ, Dai B, Zhou ZL, Wang RQ, AMPK: an energy sensor for non-small cell lung cancer progression and treatment, Pharmacol. Res. 212 (2025) 107592. [PubMed: 39805353]

[75]. Ishikawa K, Takenaga K, Akimoto M, Koshikawa N, Yamaguchi A, Imanishi H, Nakada K, Honma Y, Hayashi J, ROS-generating mitochondrial DNA mutations can regulate tumor cell metastasis, Science 320 (2008) 661–664. [PubMed: 18388260]

[76]. Piskounova E, Agathocleous M, Murphy MM, Hu Z, Huddlestun SE, Zhao Z, Leitch AM, Johnson TM, DeBerardinis RJ, Morrison SJ, Oxidative stress inhibits distant metastasis by human melanoma cells, Nature 527 (2015) 186–191. [PubMed: 26466563]

[77]. Papandreou I, Cairns RA, Fontana L, Lim AL, Denko NC, HIF-1 mediates adaptation to hypoxia by actively downregulating mitochondrial oxygen consumption, Cell Metab. 3 (2006) 187–197. [PubMed: 16517406]

[78]. La Vecchia S, Sebastian C, Metabolic pathways regulating colorectal cancer initiation and progression, Semin. Cell Dev. Biol. 98 (2020) 63–70. [PubMed: 31129171]

[79]. Zhang Y, Sun M, Zhao H, Wang Z, Shi Y, Dong J, Wang K, Wang X, Li X, Qi H, Zhao X, Neuroprotective effects and therapeutic potential of dichloroacetate: targeting metabolic disorders in nervous system diseases, Int. J. Nanomed. 18 (2023) 7559–7581.

[80]. Morten KJ, Beattie P, Brown GK, Matthews PM, Dichloroacetate stabilizes the mutant E1alpha subunit in pyruvate dehydrogenase deficiency, Neurology 53 (1999) 612–616. [PubMed: 10449128]

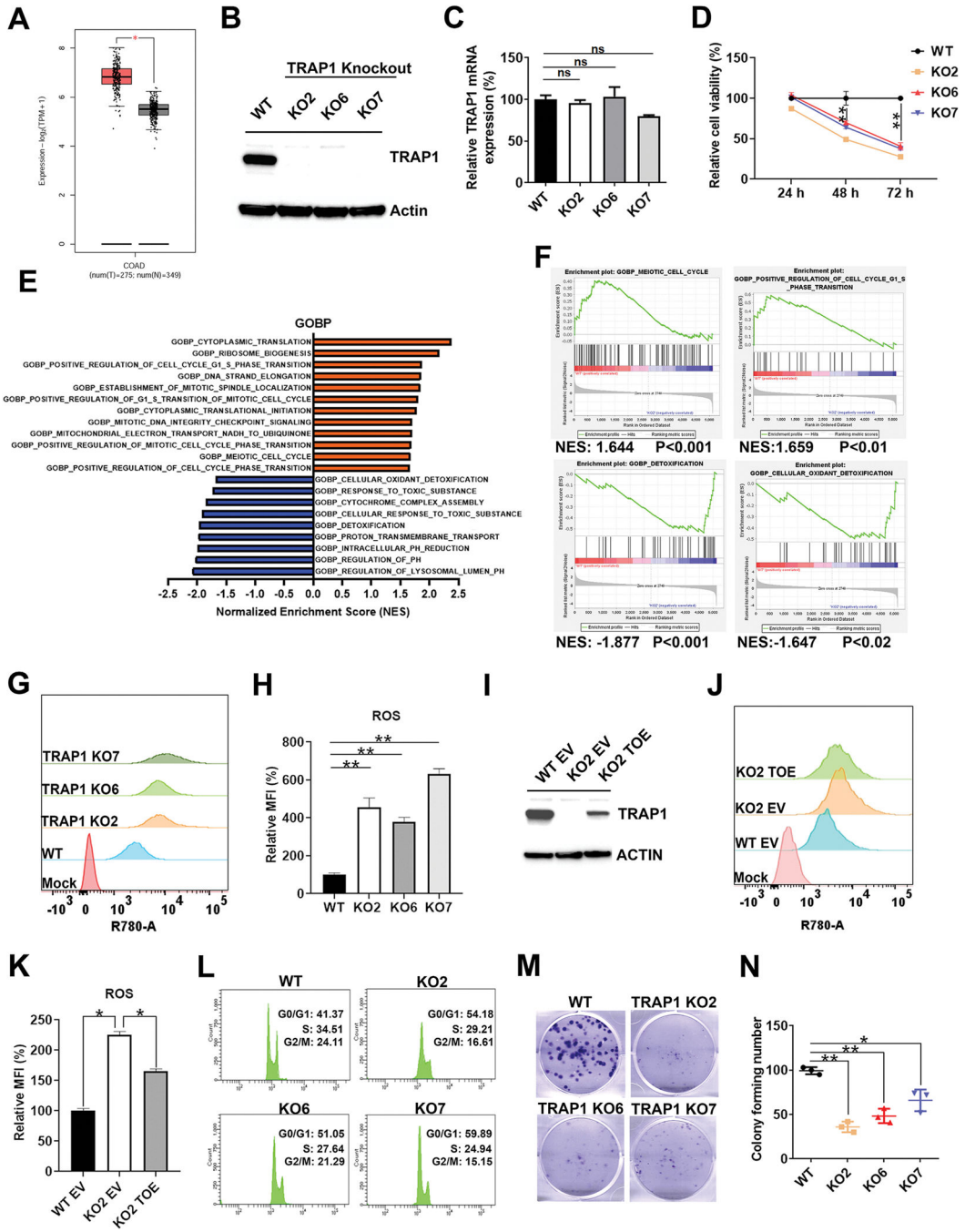

Fig. 1. TRAP1 is essential in maintaining colon cancer survival and redox homeostasis.

(A)TRAP1 expression levels in normal versus colon tumor tissues, according to the TCGA database, as displayed on the GEP2 website. (B) TRAP1 protein expression was not detectable in TRAP1 CRISPR/Cas9 CT26 cells using Western blot analysis. (C) TRAP1 mRNA levels were quantified by qPCR in WT and KO colon cancer cells. (D) Cell growth of WT and KO cells was measured at 24 h, 48 h, 72 h using CCK-8. (E) GSEA of proteomic data using Molecular Signatures Database (MSigDB) GO BP gene set is summarized as the normalized enrichment score (NES) in WT and KO cells. (F) GSEA plots of cytoplasm

translation, regulation of cell cycle G1-S, detoxification and cellular oxidant detoxification gene signatures that are associated with depletion of TRAP1. (G) Intracellular ROS levels in WT and KO cells were detected using the abcam cellular ROS assay kit and analyzed by flow cytometry. (H) Quantitation of ROS. (I) Cell lysates were prepared from WT EV, KO2 EV and KO2 TOE for Western blot analysis to detect TRAP1 and Actin proteins. (J) Intracellular ROS levels in WT EV, KO2 EV and KO2 TOE were detected using an ROS assay kit and analyzed by flow cytometry. (K) Quantitation of ROS. $P < 0.05$ (*), $P < 0.01$ (**). (L) WT and individual KO cells were collected and stained with PI. The cell cycle was analyzed using flow cytometry and BD software. (M) Cells were seeded in 6-well plates and cultured for 7 days. Cells were stained with crystal violet, and colony numbers were quantified in (N).

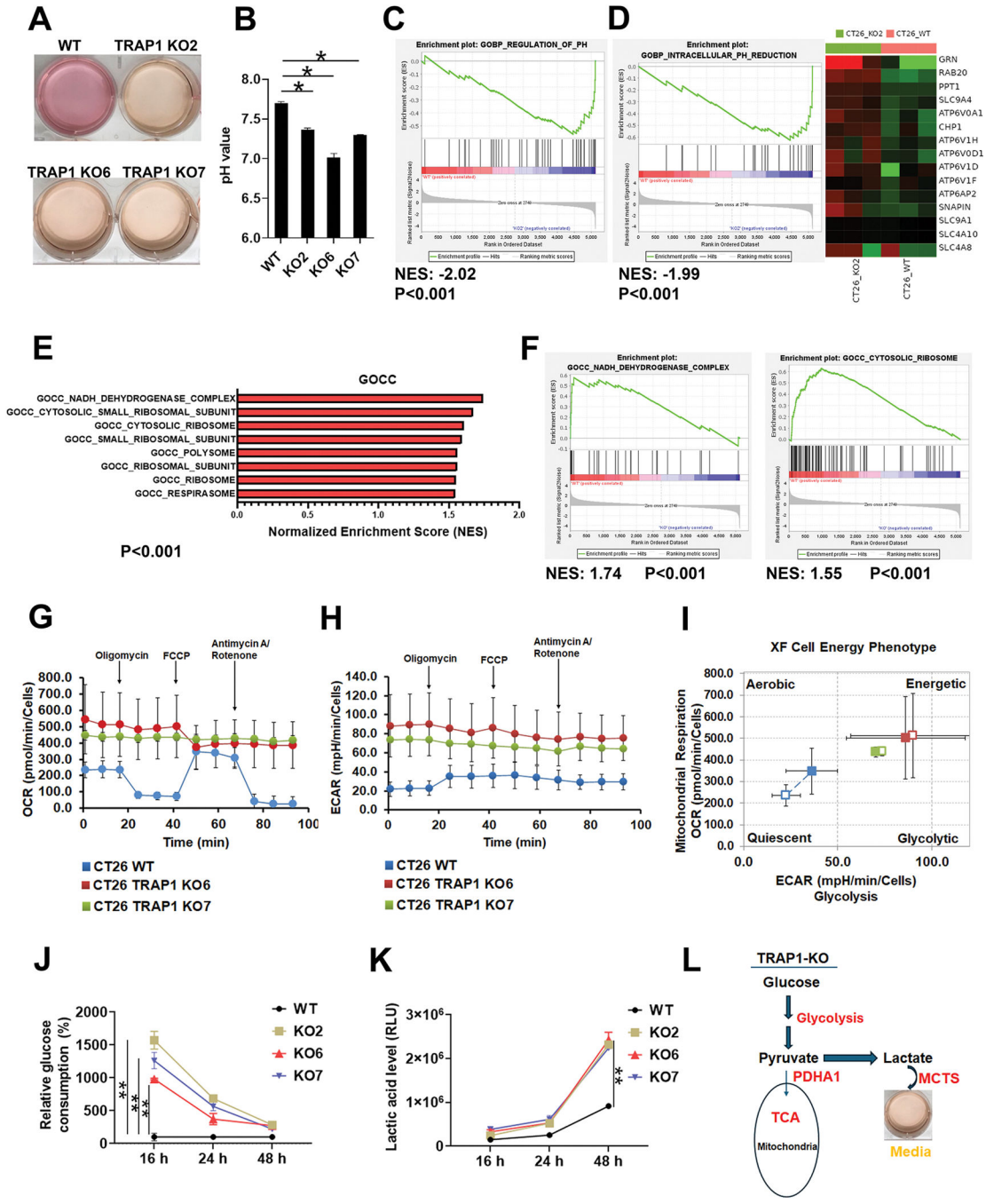

Fig. 2. Depletion of TRAP1 rewires cancer cell metabolic bioenergetics.

(A, B) The pH value of the culture medium was measured in WT and KO CT26 cells. (C, D) Enrichment analysis of proteomic data was performed using the GSEA MSigDB GO BP gene set. GSEA plots and heat maps for pH regulation genes in the TRAP1 metabolic gene signature. (E) GSEA of mass spectrometry was performed with MSigDB GO CC gene set and is summarized as the normalized enrichment score (NES) in WT and KO cells. (F) GSEA plots for NADH dehydrogenase complex and cytosolic ribosome are presented within the TRAP1 metabolic gene signature. (G, H) The oxygen consumption

rate (OCR) and extracellular acidification rate (ECAR) of WT and KO cells were measured using the Seahorse assay. The data were analyzed using Wave software. (I) The energy map generated from the Seahorse assay in WT and KO cells is shown. The empty and dotted squares represent duplicate experiments within each group. Blue indicates the WT group, red represents the KO6 group, and green represents the KO7 group. (J, K) Glucose consumption and lactate production were measured in WT and KO cells using Glucose-GLO and Lactate-GLO kits, respectively. (L) Illustration of TRAP1 depletion favors the glycolysis pathway than oxidative phosphorylation in colon cancer. $P < 0.05$ (*), $P < 0.01$ (**).

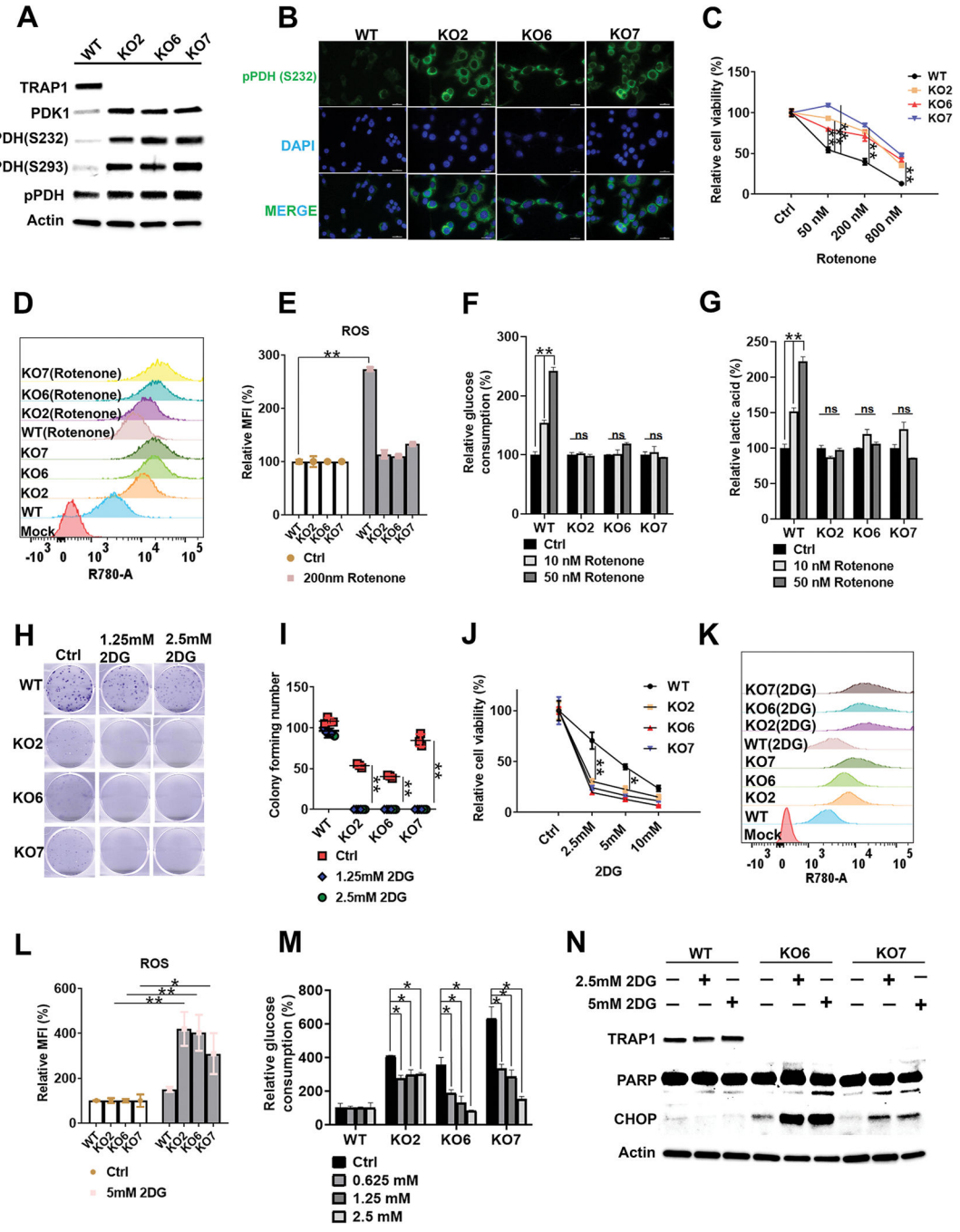

Fig. 3. TRAP1 tailor metabolic activity in colon cancer cells.

(A) TRAP1, PDK1, pPDH (S232), pPDH (S293), PDH, and Actin protein levels were detected in WT and individual KO cells using Western blot analysis. (B) WT and individual KO cells were fixed with 4 % paraformaldehyde and stained with pPDH (S232) antibody. Staining was analyzed using a Nikon microscope. (C) WT and KO cells were treated with various concentrations of rotenone for 48 h. Cell viability was determined using the CCK-8 assay at OD450. (D) Cells were treated with either Ctrl or 200 nM rotenone for 24 h. Intracellular ROS levels were detected using the abcam cellular ROS assay kit and analyzed

by flow cytometry. Quantitation of intracellular ROS levels is shown in (E). (F, G) Glucose consumption and lactate production were measured in cells treated with 10 nM or 50 nM rotenone using Glucose-GLO and Lactate-GLO kits, respectively. (H) WT and KO cells were treated with either Ctrl, 1.25 mM, or 2.5 mM 2DG for 7 days. Cells were stained with crystal violet, and colony numbers were quantified in (I). (J) WT and KO cells were treated with various concentrations of 2DG for 48 h. Cell viability was determined using the CCK-8 assay at OD450. (K) WT and KO cells were treated with Ctrl or 5 mM 2DG for 24 h. Cellular ROS levels were detected using the abcam cellular ROS assay kit and analyzed by flow cytometry. Quantitation of cellular ROS levels is shown in (L). (M) WT and KO cells were treated with 0.625 mM, 1.25 mM, or 2.5 mM 2DG for 24 h. The culture medium was collected, and glucose consumption was analyzed using Promega Glucose-GLO kits. (N) WT and KO cells were treated with various concentrations of 2DG for 48 h. Cell lysates were prepared for Western blot analysis to detect TRAP1, CHOP, PARP, and Actin protein levels. $P < 0.05$ (*), $P < 0.01$ (**).

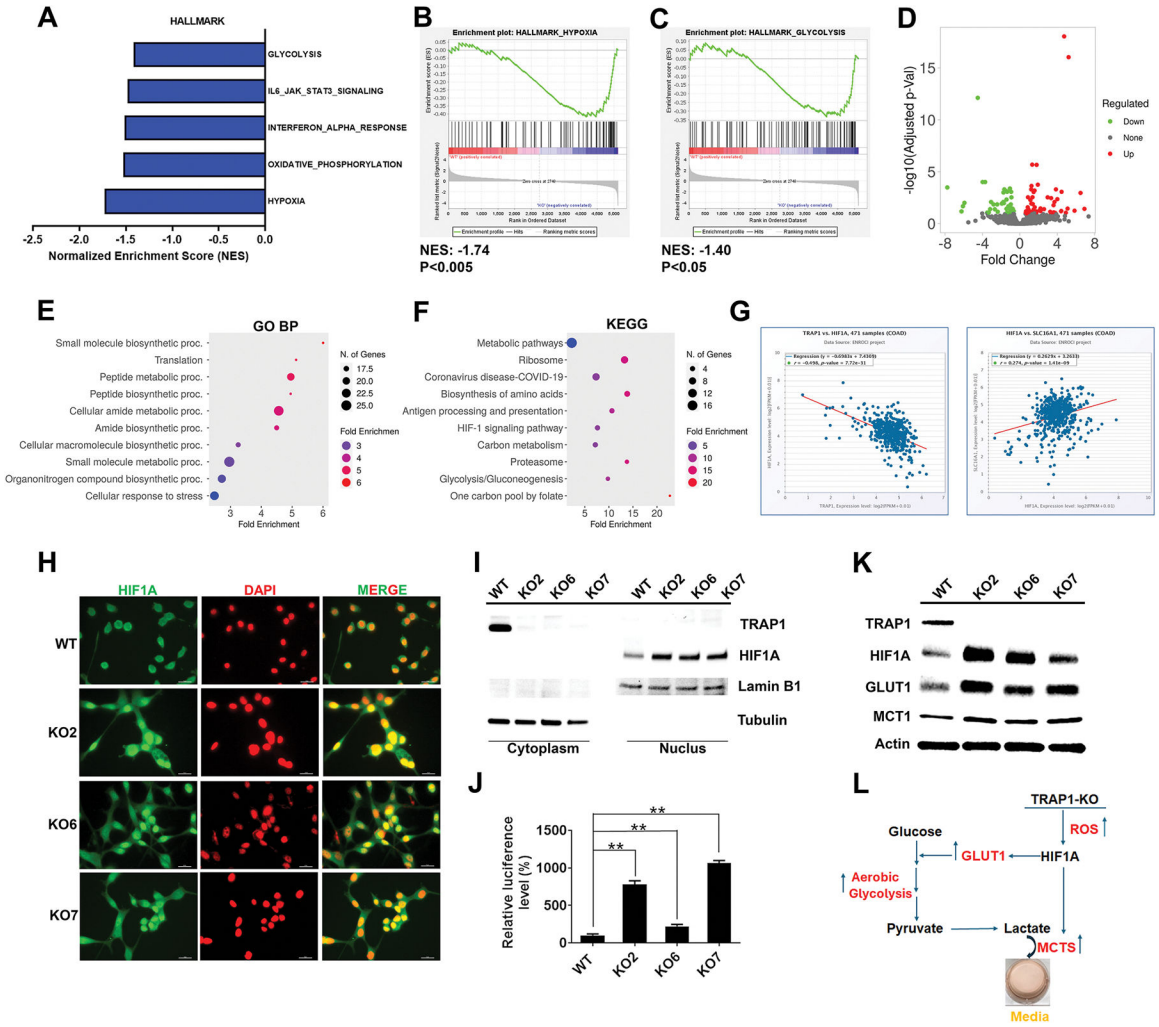

Fig. 4. Depletion of TRAP1 restricts metabolic plasticity to factitive glycolytic metabolism.

(A) GSEA of mass spectrometry was performed with MSigDB HALLMARK gene set and is summarized as the normalized enrichment score (NES) in WT and KO cells. (B, C) Enrichment analysis was carried out using the GSEA HALLMARK gene set. GSEA plots of hypoxia and glycolysis genes are presented within the TRAP1 metabolic gene signature. (D) Differential gene expressions were analyzed using DEseq2, with fold change >1.5 and FDR <0.1. Volcano plot shows relative fold change (log2) in protein abundance versus −log10(P values) from WT cells compared with KO cells. Proteins that demonstrate a significant change in expression are colored, with decreased expression in green color and increased expression in red color. (E, F) BP and KEGG pathway analysis of the differential gene expressions was conducted using ShinyGO website. The dot plot represents the top 10 significant pathways ranked according to − log enrichment P value. (G) Correlation analysis of TRAP1 with HIF1A and HIF1A with MCT1 expression in the TCGA database was performed using the ENCORI website. (H) Cells were fixed with 4 % paraformaldehyde and stained with HIF1A antibody. Staining was analyzed ushing a Nikon microscope. (I) Nuclear and cytoplasmic fractions of WT and KO cells were separated using a nuclear extraction kit (ThermoFisher). TRAP1, HIF1A, Lamin B1, and Tubulin

proteins were detected using specific antibodies by Western blotting. (J) WT and KO cells stably expressing HRE-luciferase were subjected to a reporter assay using the Promega luciferase kit, One-GLO. Luminescence levels were measured using a Luminescence reader. (K) TRAP1, HIF1A, GLUT1, MCT1, and Actin proteins were detected using Western blotting. (L) Illustration of TRAP1 depletion induces ROS generation to facilitate glycolysis pathway through ROS-HIF1A axis. $P < 0.05$ (*), $P < 0.01$ (**).

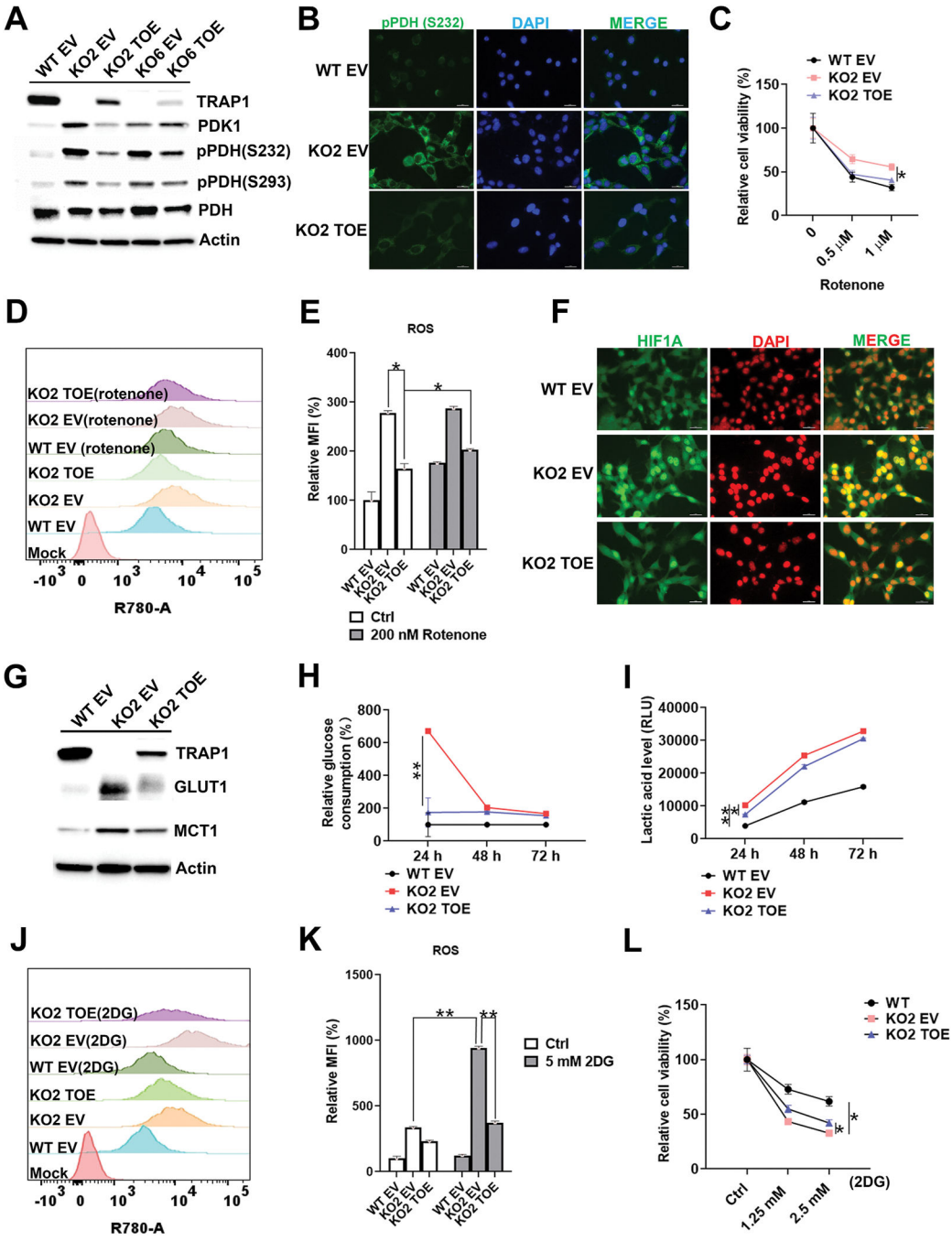

Fig. 5. Ectopic expression of TRAP1 restores PDH activity to permit metabolic plasticity.

(A) Cell lysates were prepared from WT EV, KO2 EV, KO2 TOE, KO6 EV, and KO6 TOE cells. TRAP1, PDK1, pPDH (S232), pPDH (S293), PDH, and Actin proteins were detected using Western blot analysis. (B) Cells were fixed with 4 % paraformaldehyde and stained with pPDH (S232) antibody. Staining was analyzed using a Nikon microscope. (C) Cells were treated with different dosages of rotenone for 48 h. Cell viability was analyzed using the CCK-8 assay at OD450. (D) WT EV, KO2 EV and KO2 TOE cells were treated with Ctrl and 200 nM rotenone for 24 h. Intracellular ROS levels of were detected using the abcam

cellular ROS assay kit and analyzed by flow cytometry. (E) Quantitation of intracellular ROS levels. (F) Cells were fixed with 4 % paraformaldehyde and stained with HIF1A antibody. Staining was analyzed using a Nikon microscope. (G) Cell lysates were prepared from WT EV, KO2 EV and KO2 TOE cells. TRAP1, GLUT1, MCT1, and Actin protein levels were detected using western blot analysis. (H, I) The relative glucose consumption rate and lactate concentration of the culture medium at different time points in WT EV, KO2 EV and KO2 TOE cells were measured using Glucose-GLO and Lactate-GLO kits. (J) Cells were treated with 5 mM 2DG for 24 h. Intracellular ROS levels were detected using the abcam cellular ROS assay kit and analyzed by flow cytometry. (K) Quantitation of intracellular ROS levels. (L) Cells were treated with different dosages of 2DG for 48 h. Cell viability was analyzed using the CCK-8 assay at OD450. $P < 0.05$ (*), $P < 0.01$ (**).

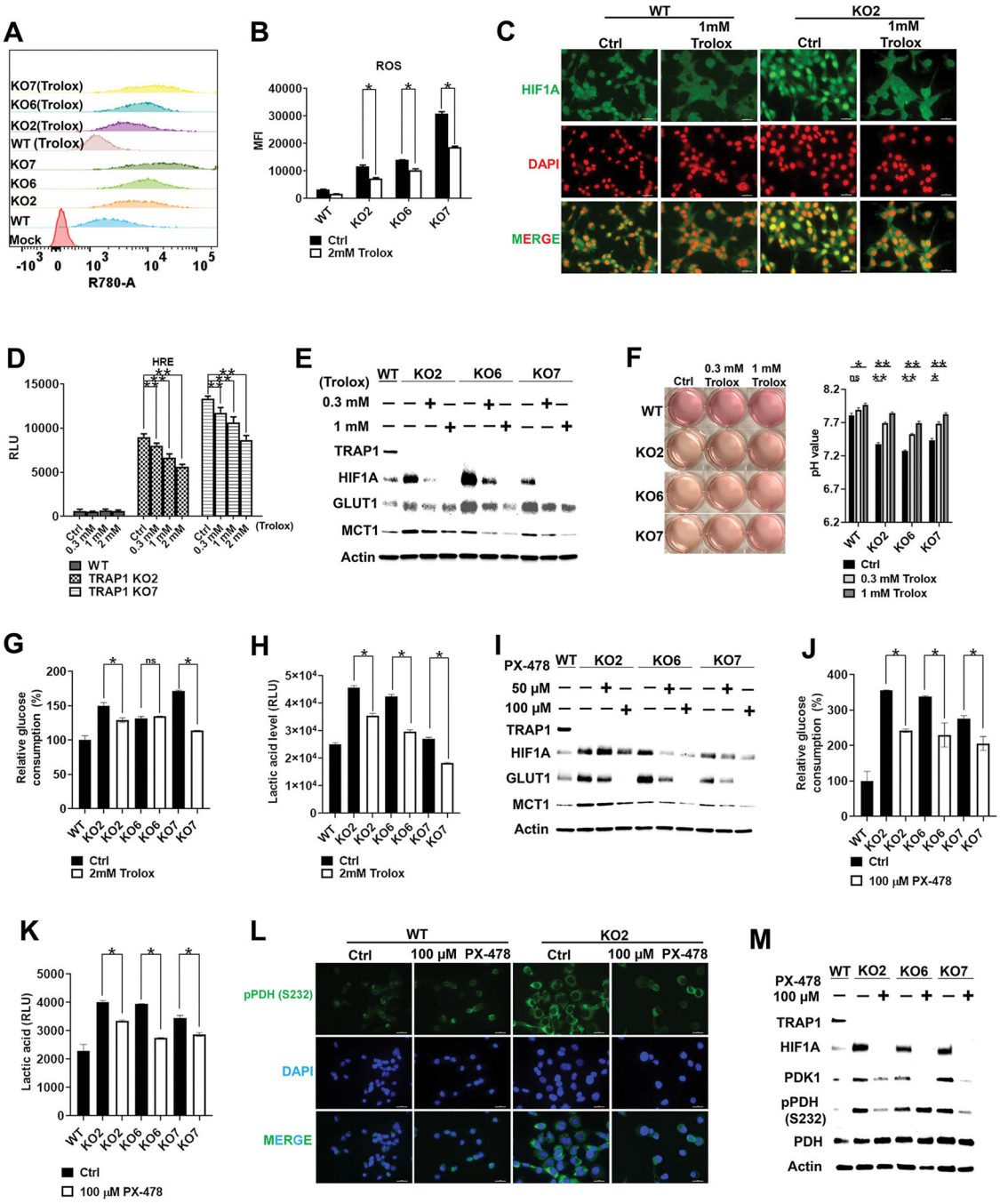

Fig. 6. ROS detoxification reverses metabolic reprogramming in KO cells.

(A) WT and KO cells were treated with 2 mM Trolox for 2 h. Intracellular ROS levels were detected using the abcam cellular ROS assay kit and analyzed by flow cytometry. (B) Quantitation of intracellular ROS levels were performed. (C) Cells were treated with Ctrl and 1 mM Trolox for 24h. Cells were fixed with 4 % paraformaldehyde and stained with HIF1A antibody. Staining was analyzed using a Nikon microscope. (D) WT and KO cells stably expressing HRE-luciferase were treated with various concentrations of Trolox for 18 h. Reporter assays were performed using One-GLO. (E) Cells were treated with 0.3 mM or 1

mM Trolox for 24 h. Cell lysates were prepared for Western blot analysis to detect TRAP1, HIF1A, GLUT1, MCT1, and Actin proteins. (F) Cells were treated with 0.3 mM or 1 mM Trolox for 48 h. The pH value of the culture medium was measured using a pH meter. (G, H) Cells were treated with Ctrl, 2 mM Trolox for 24 h. Glucose consumption and lactate production in Trolox-treated cells were measured using Glucose-GLO and Lactate-GLO kits. (I) Cells were treated with Ctrl, 50 μM, or 100 μM PX478 for 24 h. Cell lysates were prepared for Western blot analysis to detect TRAP1, HIF1A, GLUT1, MCT1, and Actin proteins. (J, K) Glucose consumption and lactate production in 100 μM PX-478-treated cells were measured using Glucose-GLO and Lactate-GLO kits. (L) Cells were treated with 100 μM PX478 for 24 h. Cells were fixed with 4 % paraformaldehyde and stained with pPDH(S232) antibody. Staining was analyzed using a Nikon microscope. (M) Cells were treated with 100 μM PX478 for 48 h. Cell lysates were prepared for Western blot analysis to detect TRAP1, HIF1A, PDK1, pPDH(S232), PDH, and Actin proteins. $P < 0.05$ (*), $P < 0.01$ (**).

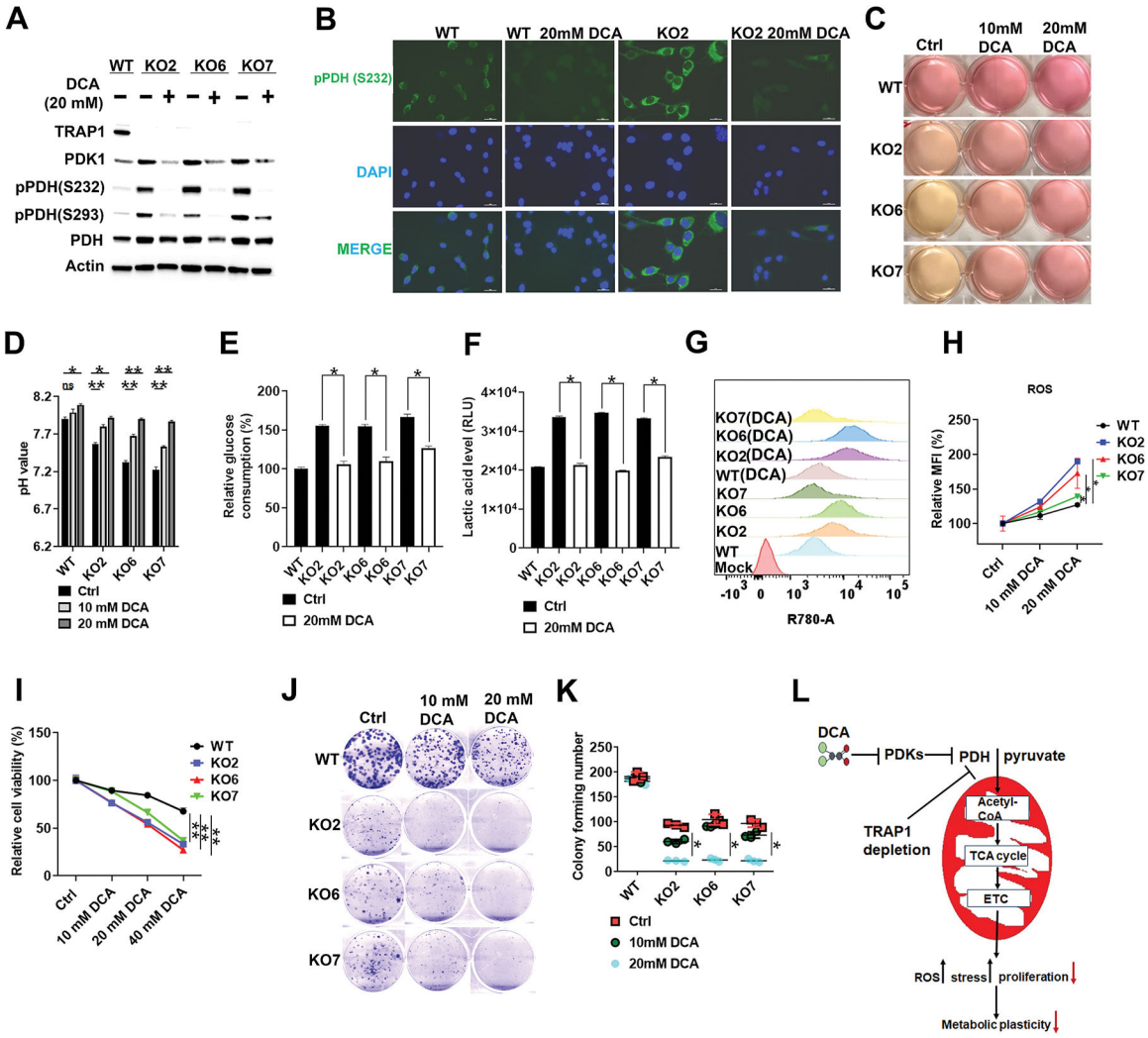

Fig. 7. Restore of PDH activity exacerbates oxidative stress and cell death in KO cells.

(A) Cells were treated with 20 mM DCA for 48 h. TRAP1, PDK1, pPDH (S232), pPDH (S293), PDH, and Actin protein levels were detected using Western blot analysis. (B) Cells were treated with Ctrl and 20 mM DCA for 24 h. Cells were fixed with 4 % paraformaldehyde and stained with pPDH (S232) antibody. Staining was analyzed using a Nikon microscope. (C, D) The pH value of the culture medium was measured in cells treated with various concentrations of DCA. (E, F) The relative glucose consumption rate and lactic acid concentration of the culture medium in DCA-treated cells were measured using Glucose-GLO and Lactate-GLO kits. (G) WT and KO cells were treated with Ctrl, 10 mM DCA, or 20 mM DCA for 24 h. Intracellular ROS levels were detected using the abcam cellular ROS assay kit and analyzed by flow cytometry. (H) Quantitation of intracellular ROS levels. (I) Cells were treated with Ctrl, 10 mM, 20 mM, or 40 mM DCA for 48 h. Cell viability was analyzed using the CCK-8 assay at OD450. (J) Cells were treated with Ctrl, 10 mM, or 20 mM DCA for 7 days. Cells were stained with crystal violet. Colony numbers were quantified in (K). (L) Illustration of the DCA activated the PDH activity to suppress cell viability in KO cells. $P < 0.05$ (*), $P < 0.01$ (**).